Identification and Characterization of 6-4 Photolyase of *Vibrio cholerae*

by

Uğur Meriç Dikbaş

A Dissertation Submitted to the
Graduate School of Sciences and Engineering
in Partial Fulfillment of the Requirements for
the Degree of

Master of Science

in

Molecular Biology and Genetics

KOÇ
UNIVERSITY

August 1, 2019

Identification and Characterization of 6-4 Photolyase of *Vibrio cholerae*

Koç University

Graduate School of Sciences and Engineering

This is to certify that I have examined this copy of a master's thesis by

Uğur Meriç Dikbaş

and have found that it is complete and satisfactory in all respects,
and that any and all revisions required by the final
examining committee have been made.

Committee Members:

_____

Prof. Ibrahim Halil Kavakli (Advisor)

_____

Assoc. Prof. Dr. Nuri Ozturk

_____

Assist. Prof. Dr. Serkan Kır

Date: _____

I dedicate this thesis to my mother, my brother Ozan, and my love Meltem…

ABSTRACT

Ultra-violet (UV) light introduces mutagenic damages to the DNA in the form of pyrimidine dimers. If not repaired, these damages may cause carcinogenic and lethal effects on the organism. Photolyases (PHRs) are the ancient flavoproteins that repair UV-induced lesions in a blue light-dependent mechanism. PHRs, according to substrate specificity, are divided into two functional groups: CPD PHRs that repair cyclobutane pyrimidine dimers (CPD) and (6-4) PHRs that repair pyrimidine-pyrimidone (6-4) photoproducts [(6-4) PP]. Although CPD photolyases are distributed among the three domains of life, (6-4) PHRs were thought to be restricted to eukaryotes. *Vibrio cholerae* (O1 bivar Tor str. N16961) possesses three cryptochrome/photolyase family (CPF) members: VcPhr, a CPD photolyase; and two single-strand CPD PHRs VcCry1 and VcCry2.

This dissertation presents the first (6-4) PHR in *V. cholerae*, named Vc (6-4) FeS-BCP. The enzyme belongs to newly discovered 'iron-sulphur cluster containing bacterial cryptochromes and photolyases' (FeS-BCP) class. Vc (6-4) FeS-BCP is the third enzyme characterized in this class. (6-4) repair activity of the Vc (6-4) FeS-BCP was demonstrated *in vitro* by DNA slot-blot repair assay. *In vivo* contribution of the protein to photoreactivation of the organism was presented by photoreactivation-complementation assay. Structural characterization of the protein via computational and experimental methods suggest that protein possesses FAD catalytic cofactor, DMRL photoantenna and [4FeS-4S] cluster.

ÖZETÇE

Ultraviyole (UV) ışık organizmaların DNAsına, pirimidin dimerleri şeklinde, mutajenik olabilecek hasarlar verir. Bu hasarlar tamir edilemezse, karsinojenik, hatta ölümcül etkilere sebep olur. Fotoliyazlar, UV-ışığın sebep olduğu bu hasaları, mavi ışığa bağlı bir mekanizmayla tamir eden antik flavoproteinlerdir. Fotoliyazlar, DNA hasarlarına göre iki fonksiyonel gruba ayrılır: siklobütan pirimidin dimerlerini tamir eden CPD fotoliyazlar ve pirimidin-pirimidon (6-4) dimerlerini tamir eden (6-4) fotoliyazlar. *Vibrio cholerae*'nın (O1 bivar Tor ırk: N16961) kriptokrom/fotoliyaz ailesine dahil üç üyeye sahip olduğu gösterilmiştir: CPD fotoliyaz olan VcPhr; ve tek iplikli DNA'ya afinitesi olan iki tane CPD fotoliyaz VcCry1 ve VcCry2.

Bu tez *Vibrio cholerae* 'da tespit edilen, ilk (6-4) fotoliyazını denysel ve hesapsal olarak göstermiştir. Bu enzim yeni keşfedilen 'demir-sülfür içeren bakteri kriptokrom ve fotoliyazları' (FeS-BCP) adlı sınıfa dahil olmaktadır. Bu çalışmada, enzimin (6-4) fotolezyonlarını tamir ettiği, *in vitro* olarak Slot-Blot DNA tamiri testi ile gösterildi. Vc(6-4) FeS-BCP'nin *Vibrio cholerae*'nın *in vivo* fotoreaktivasyonuna katkısı olduğu fotoreaktivasyon-tamamlama deneyi ile gösterildi. Yapılan yapısal ve deneysel çalışmalar Vc(6-4) FeS-BCP'nin, FAD katalitik kofaktörüne, DMRL fotoantenine ve [4Fe-4S] kümesine sahip olduğunu göstermiştir.

ACKNOWLEDGEMENTS

Firstly, I want to thank my advisor Prof. Ibrahim Halil Kavaklı. As one of the leading scientists in Turkey, his contributions to my education are priceless. I have joined to Kavaklıi Lab in 2014; since my undergraduate years, Prof. Kavaklı has always been instructive and supportive. It was a great opportunity to experience a western-quality Lab in Turkey. Words cannot express my gratitude for his trust, patience, motivation and friendly approach. I am heartily thankful to my thesis committee members Assoc. Prof. Dr. Nuri Ozturk and Asst. Prof. Serkan Kır for their scientific advices on my thesis.

I specially want to thank Dr. Nuri Ozturk. For a part of my thesis project, I joined Ozturk Lab as a guest. It was a great opportunity to learn slot-blot based DNA repair assay directly from Dr. Nuri Ozturk. I always admire his scientific thinking skills and experimental abilities. 'Dedicated to science' phrase cannot fit anybody else than Nuri Hoca. And I like to thank all members of Ozturk lab for their hospitality and friendship. I have never seen that much connected group of people.

I would like to thank Dr. Sedat Nizamoğlu and hardworking members of IDEALAB.

I also would like to thank Dr. Ibrahim Baris, Dr. Cihan Aydin and Kavaklı Lab members including Fatih Rahim. Especially, 'patron' Mehmet Tardu, Seref Gül, Cihan Aydin were not only high-skilled colleagues but also good friends/big brothers to me during these 5 years.

I want to thank my close friends who share the same destiny with me: Mehmet Eymen Sumer, Onur Sevket Taflan, Saliha Surme, Kayra Koseoglu; my lab partners Hazar Ulusoy and Gizem Parlak. I also want to thank my 'kopek' buddies: Burak Gulerce, Alp Altinoz, Firat Balkaya, Emir Bugra Gokce, Sonat Ugur, Volkan Cakir and Emre Ertekin.

Words cannot express how grateful I am to my mother and my brother, Ozan. There is no way to pay back the sacrifices they made for me.

Last but not least, I want to thank my love, my best friend, my 'pogaca' Meltem Eda Omur for her constant support and patience. Thank you for making my life beautiful with your love.

TABLE OF CONTENTS

LIST OF TABLES

LIST OF FIGURES

ABBREVIATIONS

CRY	Cryptochrome
PHR	Photolyase
UV	Ultraviolet
RMSD	Root Mean Squared Deviation
CPF	Cryptochrome/Photolyase Family
(6-4) PP	Pyrimidine-pyrimidone (6-4) photoproducts
CPD	Cyclobutane pyrimidine dimer
FAD	Flavin adenine dinucleotide
MTHF	5,10-methenyltetrahydrofolate
8-HDF	8-hydroxy-5-deazariboflavin
DMRL	6,7-dimethyl-8-ribityl lumazine
[4Fe-4S]	4 Iron – 4 Sulphur cluster
HPLC	high performance liquid chromatography
IPTG	isopropyl- β-D-1-thiogalaktopyranosid
kD	kilo Dalton
PCR	Polymerase chain reaction
CFE	Cell free extract
FRET	Fluorescence Resonance Energy Transfer
BL	Blue light
D	Dark
L	liter
h	hour
min	minute
s	second
XP	Xeroderma pigmentosum
DTT	dithiothreitol
kan	Kanamycin
amp	Ampicillin

Chapter 1:
INTRODUCTION

Exposure of DNA to UV light can introduce damages in the form of pyrimidine dimers [1]. Failure to reverse such damages may cause mutagenic, carcinogenic and lethal effects on the organism [2]. Photolyases (PHRs) are the ancient machineries that repair UV-induced lesions in a light dependent pathway. According to their substrate affinity, photolyases are functionally divided into two groups: CPD PHRs that repair cyclobutane pyrimidine dimers (CPDs) and (6-4) PHRs that repair pyrimidine-pyrimidone (6-4) photoproducts [(6-4) PPs] [3].

Possibly, due to their contribution in the earlier stages of Earth, PHRs are widely distributed among the all three kingdoms of life [4]. Cryptochromes (CRYs) are the homologs of photolyases that lost DNA repair ability and gain diverse functions ranging from circadian rhythm regulation to magnetoreception. Together, PHRs and CRYs form a family called Cryptochrome/Photolyase Family (CPF) with more than 250 members identified today.

Photolyases are flavoproteins that harvest blue-light photons and repair the UV-induced lesion in a cyclic electron transfer mechanism [5]. All photolyases contain FAD chromophore as catalytic cofactor, and an additional photoantenna chromophore in the form of MTHF, 8-HDF, FAD or DMRL. Photoantenna chromophore absorbs blue light and transfers its energy to catalytic cofactor $FADH^-$ via Förster resonance energy transfer (FRET) [6]. $FADH^{-*}$ injects an electron to the photolesion and breaks the dimer to restore two separate pyrimidines.

Vibrio cholerae O1 bivar Tor str. N16961, which will be referred as *V. cholerae* possesses three members of CPF: *Vcphr* gene encoding a CPD PHR, *Vccry1* and *Vccry2* genes encoding two single-strand CPD PHRs [7][8]. Photolyase genes are upregulated under blue light [9].

In this study, we have identified the first (6-4) photolyase in *V. cholerae* and characterize its structure and function using computational and biochemical methods. *V. cholerae* (6-4) PHR belongs to 'iron-sulfur bacterial cryptochromes and photolyases' (FeS-BCP) class [10][11] and, therefore, we named it 'Vc (6-4) FeS-BCP'. The enzyme contains universal FAD catalytic cofactor, and DMRL photoantenna chromophore

which is unique to FeS-BCP class members. Additionally, [4Fe-4S] cluster is present in the catalytic domain of the protein with a possible function in protein stability, electron transfer or DNA binding. (6-4) repair activity of the protein was shown *in vitro* by slot-blot based DNA repair assay. Contribution of the Vc(6-4) FeS-BCP to photoreactivation of *V. cholerae* cells was demonstrated in a *in vivo* photoreactivation-complementation assay. 3D structure of the protein and possible cofactors were predicted by homology modelling. Presence of the FAD and DMRL cofactor was supported by spectroscopic analysis.

Chapter 2 gives an elaborative review on UV-induced DNA damages and photolyase-mediated photolesion repair.

Chapter 3 explains the materials and methods used in the study.

Chapter 4 presents the results of the study. Identification and purification of the protein were explained. Spectral characteristics and predicted 3D structure of the protein were demonstrated. Repair activity of the purified protein and the effect of the protein on photoreactivation *in vivo* has been shown.

Chapter 5 and Chapter 6 concludes the thesis and addresses the future directions for the study.

Chapter 2:
LITERATURE REVIEW

In 1949, Albert Kelner suggested that visible light has a component that resurrects *Streptomyces griseus* cells after becoming non-viable by UV light irradiation[12]. Mystery underlying the reversal of UV induced damage by a lower-energy light attracted many physicists to the field including Dr. Claud Stan Rupert. Dr. Rupert knew that photoreactivating machinery was not possessed by all life forms. While, *E. coli* cells had photoreactivation capability, *H. influenzae* strain were not able to reverse UV induced DNA damage with visible light. Using this information, Dr. Rupert designed a *Haemophilus* transformation assay to analyze molecular basis of this phenomenon, called photoreactivation. He illuminated UV light on DNA isolated from *H. influenzae* and observed a significant decrease in transformation efficiency. Then, he mixed UV inactivated transforming DNA with *H. influenzae* or *E. coli* cell free extract and kept under either light or dark conditions. He observed that inactivated DNA was reactivated only when mixed with *E. coli* cell free extract and illuminated with light, suggesting a cellular factor in *E. coli* CFE harvests light to reactivate cells[13]. Photoreactivation phenomenon was directly proportional to the light intensity and the cell free extract amount; and, reactivating capacity was vanished when cell free extract heated to 90 °C. His findings marked year 1958 as the first photolyase studies and opened a field in biology as DNA repair.

In the early 1960s, it was discovered that UV light caused dimerization of thymine in a frozen aqueous thymine solution in the form of cyclobutane pyrimidine dimer [14][15]. Later, Dr. Rupert's team showed that the yeast photoreactivating enzyme specifically interacts with unrepair DNA to form enzyme-substrate complex and the repair reaction follows Michaelis-Menten kinetics [16][17]. In fact, due to low number of photolyases in one cell (around 20 protein molecules in one cell), it was hard to understand the molecular mechanism in depth. In 1974, 2105 Chemistry Nobel Laurate Prof. Aziz Sancar joined to Rupert Lab and cloned *E. coli* photolyase gene into a plasmid [18]. Overexpressed and purified protein exhibited dark blue color indicating light absorbing property of the protein itself. Cloning of the *E. coli* PHR into a plasmid not only led to understanding photolyases' molecular mechanism, but also enabled

scientists to discover other DNA repair machineries such as nucleotide excision repair (NER).

2.1 UV Light and DNA Damage

10 nm – 400 nm region of electromagnetic spectrum is designated as UV radiation which contributes around 10% of Sun's total output. UV range corresponds to the wavelengths shorter than visible light and longer than X-rays. UV radiation - according to their wavelength- can be both beneficial and harmful. Shorter wavelengths of UV light including UV-C (100-280 nm) can cause chemical reactions and therefore biological harms if not filtered out by the atmosphere.

Shorter wavelengths of UV-C and more-energetic bands of solar UV are absorbed by oxygen in the atmosphere. Oxygen molecules (O_2) absorbing high-energy UV light splits into freed oxygen atoms and later forms the ozone molecules (O_3) in the ozone layer. UV-C's wavelengths that are not filtered by oxygen molecules and a significant part of UV-B are blocked by the ozone layer. So that, UV-C is completely absorbed by Earth's atmosphere or ozone layer and -in a cloudy day- around 90% of UV-B is filtered by ozone layer. UV-B (280-315 nm) is considered as intermediate UV. While UV-B has positive effects such as conversion of 7-dehydrocholesterol into vitamin D in the skin, overexposure of UV-B may increase the risk of skin cancer. Near-violet UV light which is not absorbed by ozone layer is termed as UV-A (315-400 nm). UV-A can penetrate the depths of the sea and has variety of functions in biological process such as DNA repair.

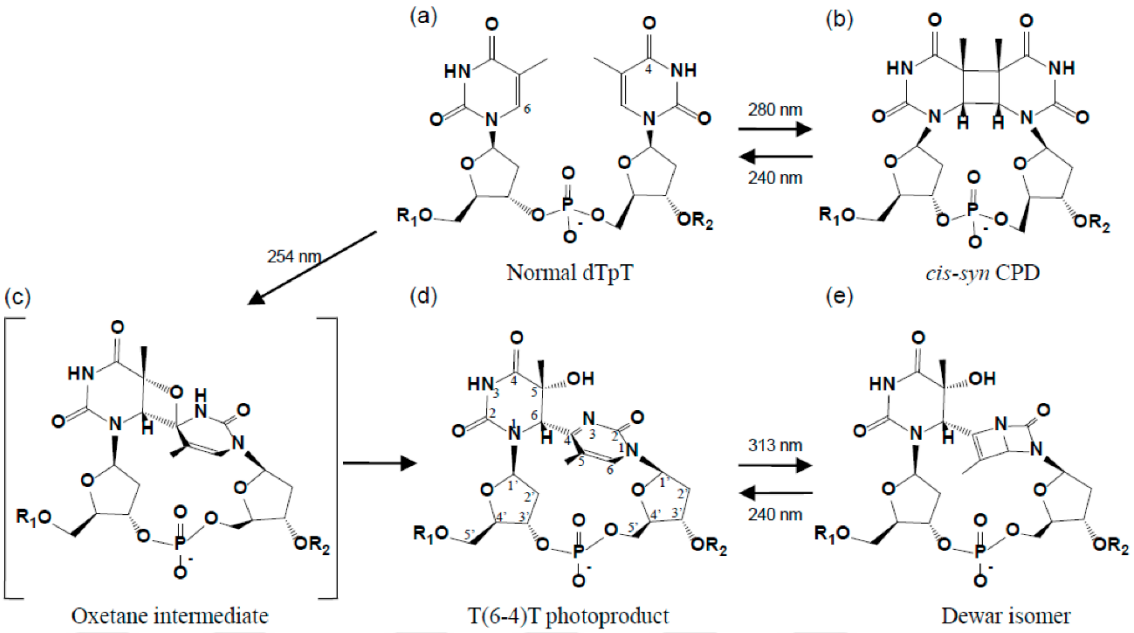

Figure 1. *Chemical structure of UV-induced DNA lesions. (a) Normal thymidine dimer, (b) cis-syn CPD, (c) oxetane intermediate, (d) (6-4) thymidine dimer and (e) Dewar isomer. (Reprinted from the reference* [19] *with permission)*

UV light introduces damages to the double stranded DNA which subsequently may lead to mutations, growth delay, cellular transformation and cell death. UV induced photoproducts occur between two adjacent pyrimidines (same strand), mostly in the form of cis-syn cyclobutane pyrimidine dimers (CPDs), pyrimidine-pyrimidone (6-4) photoproducts and Dewar isomers (Figure 1). ~80% of the total photoproducts corresponds to CPD and the remaining ~20% corresponds to (6-4) PPs. CPDs are formed by a [2π + 2π] cycloaddition reaction between two adjacent C5=C6 double bonds[14][20], while (6-4) PPs are generated by a Paternò–Büchi reaction between the C4 carbonyl group of a 3’ pyrimidine and the C5=C6 double bond of a 5’ pyrimidine[21][19]. Both types of photoproducts may form between any combination of two adjacent pyrimidines: 5’-T-T-3’, 5’-T-C-3’, 5’-C-T-3’ and 5’-C-C-3’, except 5’ cytosine (6-4) photoproducts are least favorable [22]. Douki et. al. represents the formation frequencies of different photoproducts under UV-B and UV-A via a HPLC-MS/MS based quantification method (Figure 2) [23]. (6-4) PPs are premutagenic, causing specifically 3’T-to-C transitions during replication [24][25]. If these mutations are introduced to the genes that are functioning in the programming of cell proliferation and apoptosis, they may promote carcinogenesis.

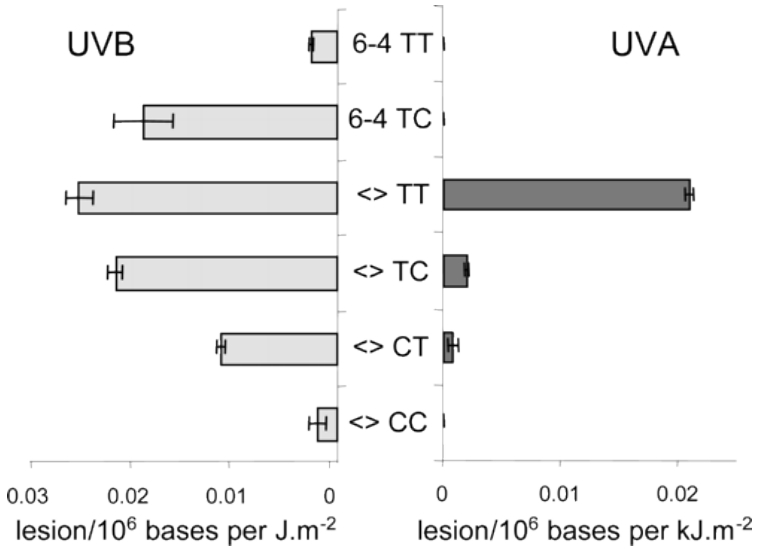

Figure 2. The yield of pyrimidine dimer formation frequencies under UVa and UVb light. (Reprinted with permission from T. Douki, et al. [23]*. Copyright (2003) American Chemical Society)*

2.2 Photolyase

Photolyases are the molecular machineries that uses blue light energy to repair UV induced pyrimidine dimers. Probably due to their contributions to survival of the organisms in the earlier stages of Earth, photolyases are highly distributed to all three kingdoms of life [26]. In their general structure, photolyases contain two chromophores: FAD that function as catalytic cofactor and a photoantenna such as MTHF,8-HDF or DMRL. Recently discovered FeS-BCP class (6-4) photolyases also contain a cubane-type [4Fe-4S] cluster with a possible function in DNA binding, protein stability or electron transfer [10][11]. An *E. coli* cell contains around 16-17 photolyase molecules that scan the DNA[27][28]. As an overall mechanism, photolyases non-covalently interacts with pyrimidine dimers and flips the lesion into the DNA in a light independent manner [29]. Photoantenna chromophore absorbs blue/near-UV light and transfers the excitation energy to catalytic cofactor via FRET. Catalytic cofactor $FADH^-$, then, transfers an electron to photolesion and splits two pyrimidines in a cyclic reaction.

2.2.1 Protein Structure

Photolyases are monomeric globular proteins with a size of 45-66 kDA and with a length of 420-616 amino acids[26]. The holoenzyme contains two cofactors: FAD and a

photoantenna chromophore. FAD catalytic cofactor is universal to all photolyases identified up to now, and essential for lesion binding and catalytic activity[22]. The second cofactor is a light harvesting chromophore generally in the form of deazaflavin such as 8-HDF, pterin such as MTHF; or DMRL. Photoantenna chromophore is not essential for photolyases. Site-directed mutagenesis studies revealed that PHRs lacking photoantenna are still active, but with a lower repair efficiency [30].

Crystal structures of several photolyases have been determined and available in Protein Data Bank (PDB). Although, sequence identities between photolyases can be as low as 25%, a well-defined general architecture is shared by all members[31]: an N-terminal α/β domain is connected to C-terminal α-helical domain with an inter-domain binding loop (Figure 3). The crystal structures of *E. coli* PHR and *A. tumefaciens* PhrB will be discussed as representatives of CPD and (6-4) photolyases, respectively.

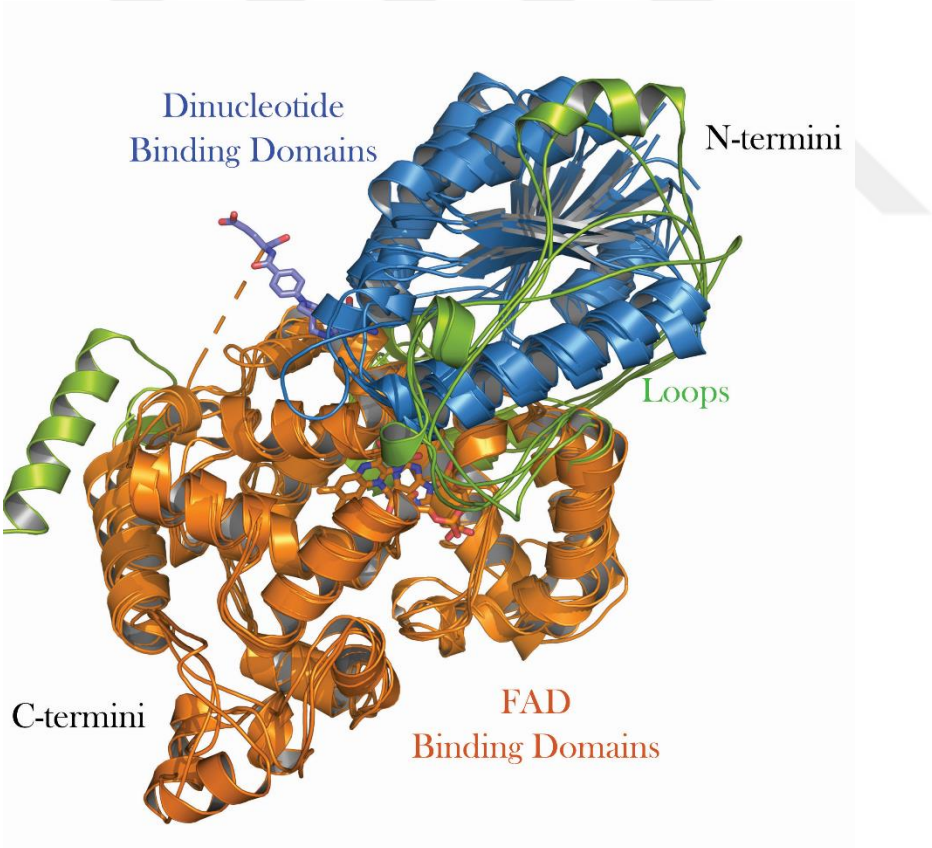

Figure 3. Superimposition of structures of different photolyases. Superimposition of E. coli PHR, T. thermophilus CPD PHR, A. nidulans CPD PHR and A. thaliana (6-4) PHR is demonstrated in cartoon representation. Catalytic domain (C-termini) and photoantenna binding domain (N-termini) are colored in orange and blue, respectively. Interdomain loop is shown in green. (Reprinted from the reference [2]*. Copyright (2019) with permission from Elsevier)*

In 1995, 3D crystallographic structure of *E. coli* photolyase is presented by Park et al. at a resolution of 2.3 Å (Figure 4a) [32]. Protein's 1-131 residues correspond to the α/β domain and 204-472 residues correspond to α-helical domain. Two domains are connected via a long loop (132-203 residues) surrounds the α/β domain. Light harvesting cofactor, MTHF, is located in a cleft between two domains where it has an accessibility to light source while FAD catalytic cofactor is deeply buried in α-helical domain in an unusual U-shaped conformation. The distance between two cofactors is 16.8 Å and the transitional dipole moments of MTHF and $FADH^-$ are oriented with 90º angle; these structural characteristics of *E. coli* photolyase favors the energy transfer from MTHF to $FADH^-$ via FRET (with ~70% efficiency) [31][32]. Surface potential representation of the protein (Figure 4b) reveals a hole that leads to $FADH^-$ cofactor in a positively charged grove. Later, the hole is shown to accommodate CPD lesion in the co-crystal structure of *Anacystis nidulans* CPD photolyase with CPD photoproduct [29].

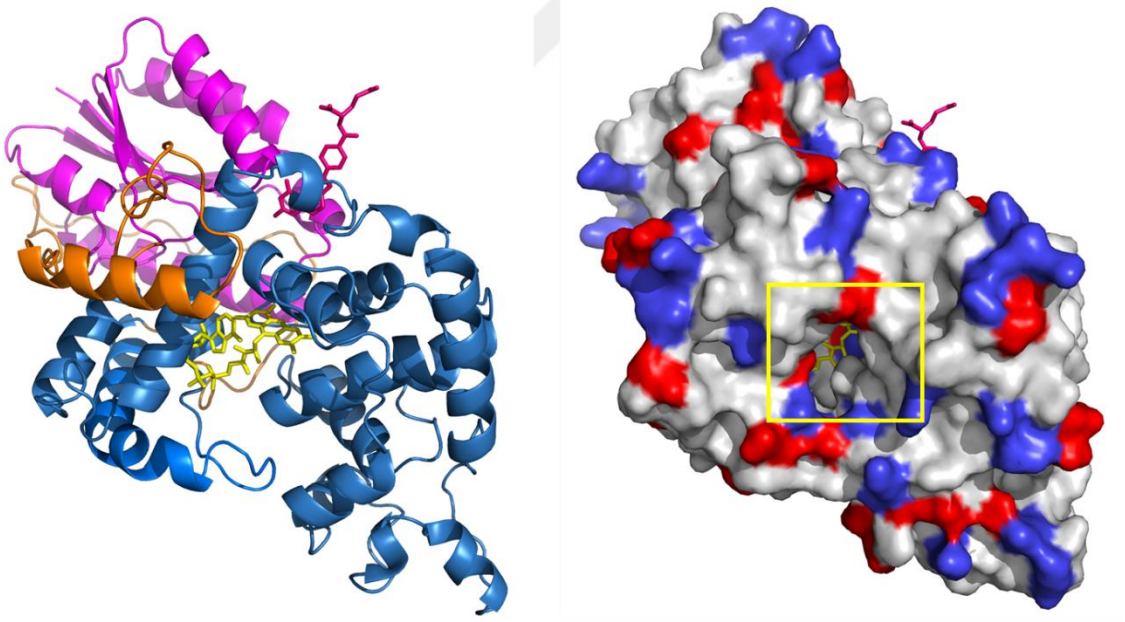

Figure 4. Crystal structure of E. coli PHR (PDB ID: 1DNP) [32]. *(a) Cartoon representation of E. coli PHR. α-helical domain and α/β domain are colored in blue and pink, respectively. Orange color indicates the interdomain loop. MTHF (magenta) is located in a cleft between two domains and sticks out. FAD (yellow) is located in the catalytically active site of the enzyme. (b) Surface representation of E. coli photolyase. Positively charged amino acids are colored red and negatively charged amino acids are shown in red. Yellow box highlights the cavity that leads to FAD catalytic cofactor.*

Long after the discovery of CPD PHRs, the first (6-4) photolyase was identified in *Drosophila melanogaster* by Todo et al., in 1993[33][34]. 20 years long, (6-4) photolyases were thought to restricted to eukaryotes. In 2013, Zhang et al. presented evidence for (6-4) repair activity of *Agrobacterium tumefaciens* PhrB and determined the crystal structure of the protein at 1.45 Å resolution [11]. PhrB belongs to a new class of Cryptochrome/Photolyase family: FeS-BCP [35]. It contains FAD catalytic cofactor, a DMRL photoantenna chromophore and a cubane-type [4Fe-4S] cluster. Considering all the CPF members identified today, DMRL cofactor and [4Fe-4S] cluster are only conserved in FeS-BCP class of Cryptochrome/Photolyase family [2].

Figure 5 represents the overall crystal structure of PhrB (4DJA) and cofactor arrangements [11]. The model structure contains 21 α helices, 5 β sheets and 5 3_{10} helices. 5 β sheets and 5 α helices (α1 to α5) corresponds to N-terminal α/β domain (residues 2-127). α/β domain's structural motif resembles a typical Rossman nucleotide binding fold [36]. DMRL is located in this domain and proposed to function as light-harvesting photoantenna. α9 to α21 helices and all 5 3_{10} helices form the second domain: C-terminal α-helical domain (residues 231-512). The α-helical domain contains [4Fe4S] cluster and FAD cofactor and corresponds to the catalytic region of the enzyme. The antenna binding domain and catalytic domain are connected by an interdomain loop (residues 128-230). Interestingly, FeS-BCP members showed the least homology with their counterparts in eukaryotic organisms, Drome (6-4) PHR (RMSD: 3.2 Å) and Arath (6-4) PHR (RMSD: 3.5 Å), suggesting their separation in the earlier stages of CPF evolution path [11].

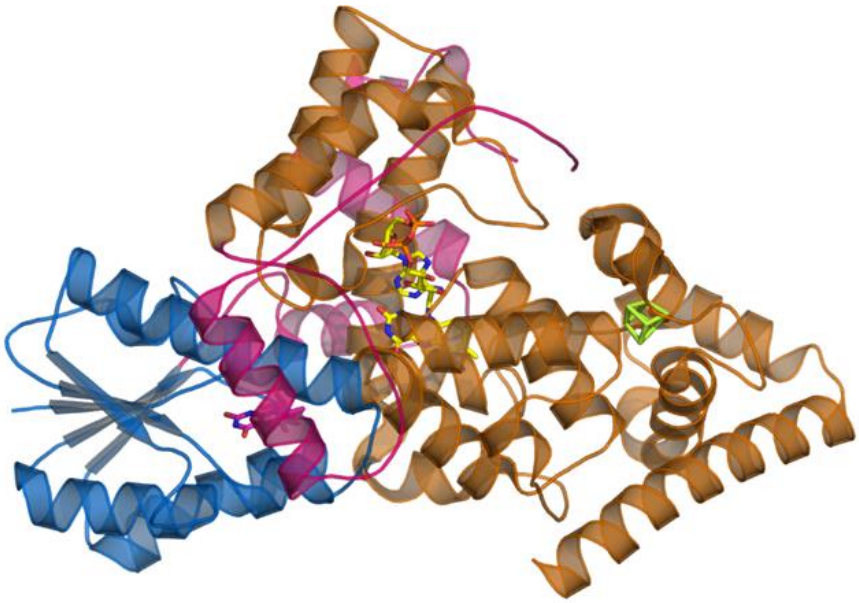

Figure 5. Overall structure of A. tumefaciens PhrB (PDB ID: 4DJA) [11]. *Photoantenna binding domain (blue), catalytic domain (orange) and interdomain loop (pink) are shown in cartoon representation. PhrB contains FAD catalytic cofactor (yellow), DMRL (magenta) and [4Fe-4S] cluster (green).*

2.2.2 FAD Catalytic Cofactor and Photoreduction

All photolyases comprise FAD as a light sensitive catalytic cofactor. Upon excitation, FAD transfer an electron to the DNA lesion and splits pyrimidine dimers in a radical mechanism[26]. FAD is buried into the α-helical domain and appears in a U-shaped conformation with proximity between adenine and lumiflavin moieties to ensure intramolecular electron transfer [37]. FAD, in a prototypical photolyase, is coordinated by the interactions with 14 amino acids [31]. FAD interacting residues are highly conserved among the members of cryptochrome/photolyase family [1][38].

FAD can exist in three redox states in five different forms: the oxidized form (FAD), semireduced semiquinones (anion radical $FAD^{\bullet -}$, neutral radical $FADH^{\bullet}$) and fully reduced hydroquinone ($FADH^{-}$, $FADH_2$) (Figure 6a)[39][40]. All three redox states of FAD have a part of absorption band that overlaps with the emission of MTHF chromophore, allowing energy transfer from MTHF to FAD (Figure 6b)[41]. However, the intramolecular electron transfer dynamics in different redox states of FAD revealed that $FADH^{-}$ is the only active state in DNA repair[37]. For experimental purposes, fully oxidized FAD or neutral semiquinone $FADH^{\bullet}$ can be reduced to its active $FADH^{-}$ form by illumination in a solution containing reducing agents such as DTT.

The photoreduction of FAD to its fully reduced form is called photoactivation [42]. *In vitro* photoactivation process requires two steps: (1) the photoexcitation of FAD and (2) the electron transfer from the protein's surface to the FAD.

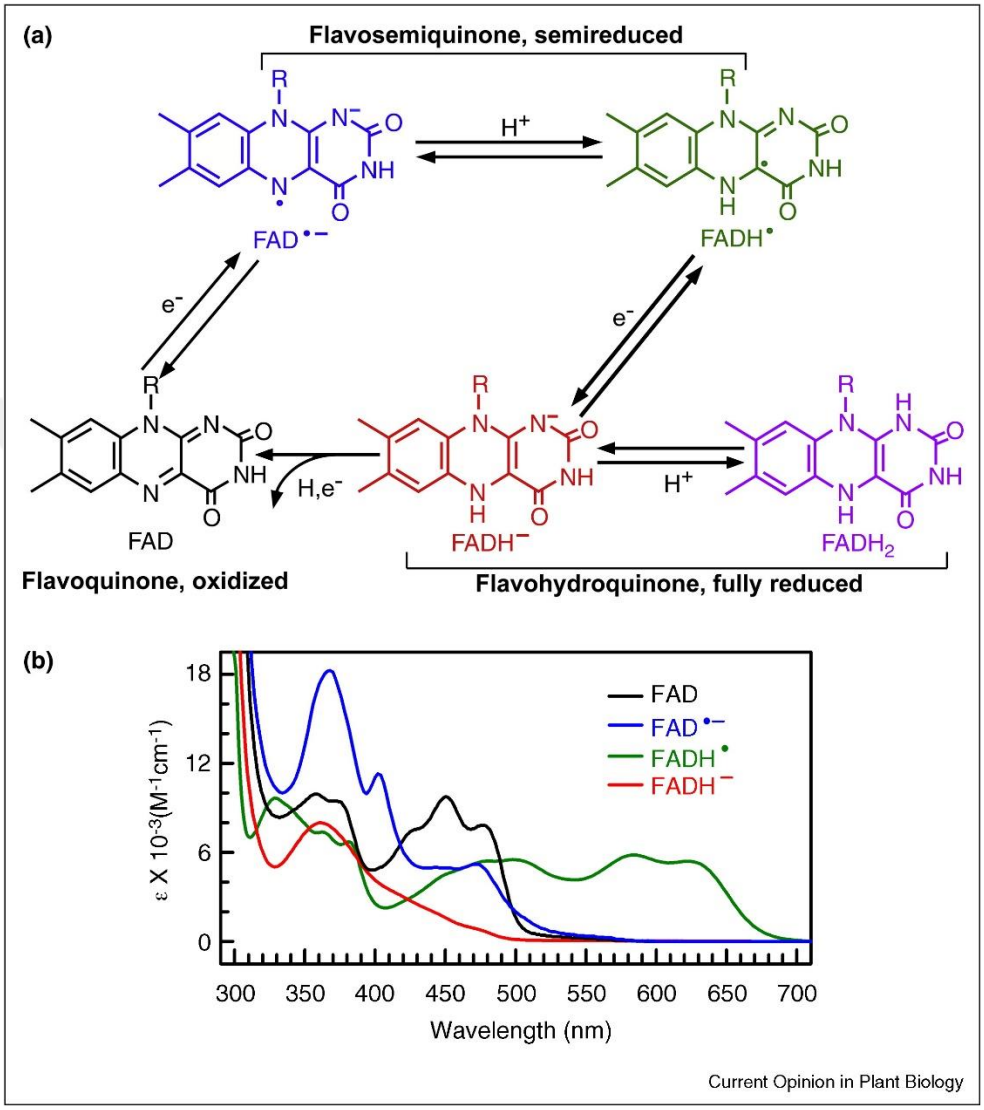

Figure 6. Redox states of FAD. (a) Five redox forms of FAD and (b) absorption spectrum of different redox states. (Reprinted from Liu et al.[39]*. Copyright (2010) with permission from Elsevier)*

FAD can obtain the energy required for photoactivation in either via direct blue light photon absorption or FRET from the antenna chromophore. Resonance energy transfer from antenna chromophore to catalytic domain will be discussed in "Photoantenna Chromophore" section.

Electron transfer dynamics during photoreduction of fully oxidized FAD [43] and semiquinone $FADH^{\bullet}$ [44] has been studied in MTHF lacking *E. coli* PHR (E109A) at femtosecond resolution. Photoreduction mechanism can be summarized as follows: Upon the excitation, $FADH^{\bullet}$ attracts the electron flow and initiates an electron hoping cascade from the protein surface to $FADH^{\bullet}$ along the three highly conserved tryptophan residues, called Trp triad (W382, W359, and W306 in *E. coli* PHR) (Figure 7a) [42][45][44]. Surface-exposed tryptophan residue (W306), then, stabilizes the reduced cofactor by accepting one electron from the reducing agent in the solution. Mutation on W306 abolishes photoreduction of $FADH^{\bullet}$ [46]. Photoreduction of oxidized FAD includes two additional tryptophan residues: W384 and W316 (Figure 7b) [43]. W382 of Trp triad, W384 and adenine moiety of FAD have direct electron transfer with flavin and form the first layer of electron transfer. W316 and W359 constitutes the second layer, W306 forms the solvent exposed third layer. Photoreduction efficiency is achieved by fast electron transfer to active site (less than 150 ps) and slow reverse electron flow (in nanoseconds)[43]. Except Class II photolyases and FeS-BCPs, the Trp triad is highly conserved in photolyases. However, *in vivo* study suggested that photoreduction is not part of the reaction mechanism for photolyases [28].

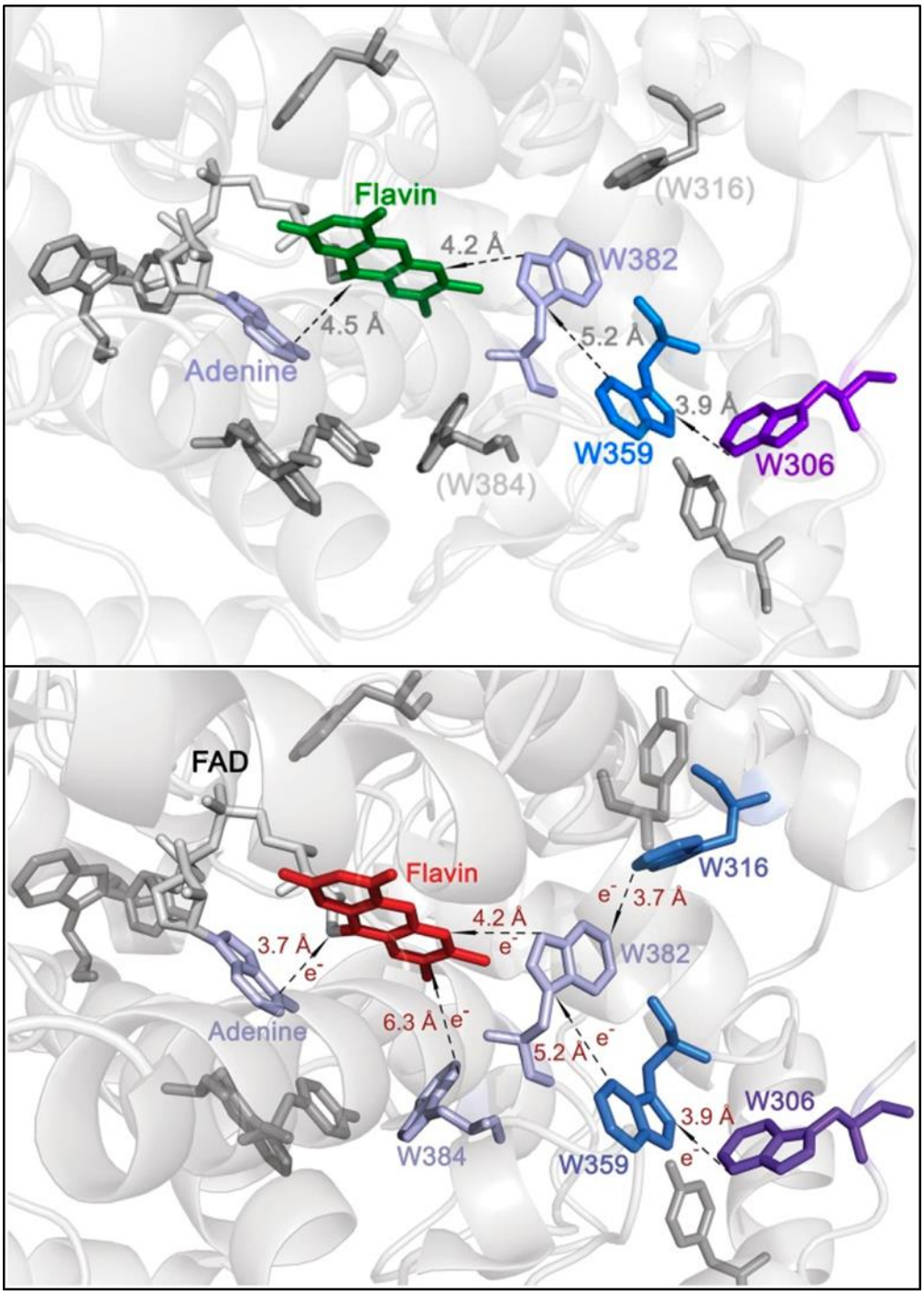

Figure 7. In vitro photoreduction of FAD. (a) semiquinone FADH• [43] *and (b) fully oxidized FAD* [44] *are photo-reduced through a highly conserved Trp-triad. Photoreduction of oxidized FAD includes two additional tryptophan residues. First layer of the ET is colored as light purple. Second layer and third layer of the ET are shown in blue and dark purple respectively. (Reproduced from the reference* [5] *with permission of ANNUAL REVIEWS in the format Thesis/Dissertation via Copyright Clearance Center)*

2.2.3 Photoantenna Chromophores and Photoinitiation

The second chromophore of photolyases serves as the light-harvesting photoantenna. Even though they are not essential for photolyases, they enhance the light absorption efficiency and subsequently DNA repair efficiency. In general, photoantenna chromophores have larger extinction coefficient and broaden photolyases' activity spectrum [5]. MTHF and 8-HDF are the two common photoantenna chromophores associated with CPD photolyases [1]. The energy transfer between two chromophores is achieved by Förster resonance energy transfer via long-range dipole-dipole interactions [5]. Energy transfer from MTHF photoantenna to FAD cofactor has been extensively studied in *E. coli* PHR[47][48][41], *V. cholerae* VcCry1 [6] and Class III CcPL [49] by measuring the dynamics of MTHF fluorescence quenching. Elimination of the energy acceptor (FAD) in *E. coli* PHR by site directed mutagenesis gave further accuracy in measuring the dynamics of excited MTHF and enabled the capturing of intermediates formed through energy transfer [41].

Other than MTHF and 8-HDF, FMN chromophore in *Thermus thermophilus* photolyase [50] and FAD in *Sulfolobus tokodaii* photolyase [51] have been described as antenna chromophores. Eukaryotic (6-4) photolyases studied to date only contain 8-HDF [52] as the second cofactor. Additionally, recent structural studies on *Rhodobacter sphaeroides* CryB and *Agrobacterium tumefaciens* PhrB revealed a new photoantenna chromophore: DMRL[10][11]. DMRL, also notated as DLZ, is the last intermediate of the riboflavin biosynthesis pathway [53]. DMRL is also found in fluorescent accessory protein, LumP, of luminous marine bacterium, *Photobacterium kishitanii*. DMRL in LumP increases the luminous strength and modulates the luciferase emission to shorter wavelengths [54].

In photolyases, photoantenna chromophore absorbs blue light photons, and transfer its energy to catalytic cofactor via FRET. Efficiency of the energy transfer increases with the decreasing intermolecular distance and it is inversely proportional to the angle between donor's and acceptor's transition dipole moments [31]. In *E. coli*. PHR, the distance between chromophores is 16.8 Å (Figure 8a) and the transition dipole moments are perpendicular to each other. While energy transfer efficiency in *E. coli*

PHR is 70% [55], *A. nidulans* photolyase has 98% efficiency with a longer interchromophore distance (17.5 Å) [56]. *A. nidulans* photolyase achieve higher efficiency by a better orientation (35.6º angle) between transition dipole moments of photoantenna and the isoalloxazine ring of FAD.

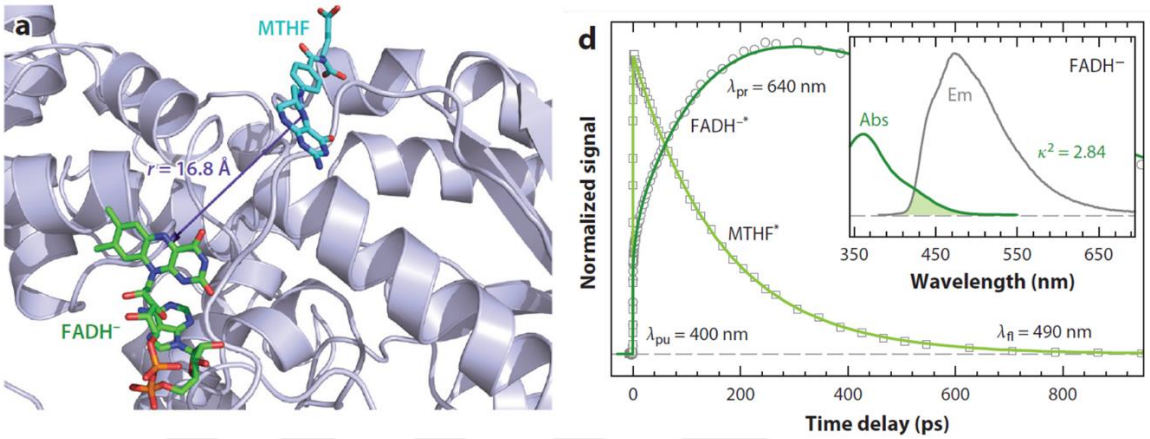

Figure 8. Energy transfer from MTHF to FADH-. (a) Crystal structure of E. coli PHR. (b) Femtosecond fluorescence and absorption transient at FADH-. Fluorescence transients reflect the MTHF 's (energy donor) quenching dynamics and absorption transients reflect the formation dynamics of FADH-* (energy acceptor). Inset shows the overlap between MTHF's emission and FADH- 's absorption spectra. (Reproduced from the reference* [5] *with permission of ANNUAL REVIEWS in the format Thesis/Dissertation via Copyright Clearance Center)*

2.2.4 Repair Mechanism

CPD photolyases are one of the first enzymes whose functional evolution and catalytic dynamics have been described at fundamental levels in real time [40]. The repair mechanism of photolyases includes a light-independent substrate-enzyme complex formation step, and three light-dependent processes: photoinitiation, photoreduction and photorepair.

Photolyases are 'structure-specific DNA binding proteins' with affinity to specific DNA lesions [1]. They recognize the backbone of the DNA duplex with UV-induced lesion without a sequence specificity [57]. Photolyases share a common positively charged DNA binding surface that leads to FAD pocket [22]. Crystal structure of *Anacystis nidulans* DNA photolyase complex with CPD analog revealed that, CPD comprising DNA (bent by 22º) is bent further to 50º and lesion is flipped into the active site of photolyase (Figure 9) [29]. In active cavity, enzyme-substrate complex is

stabilized through ionic interactions between negatively charged DNA backbone and positively charged grove on the protein surface; and weak interactions with complementary strand. Flipping out of CPD lesion into DNA binding cavity gives proximity to $FADH^-$ in which van der Waals interactions enable electron transfer during the photorepair process [1]. CPD photolyases have higher affinity to CPD lesions than undamaged/repaired DNA. For example, *E. coli* PHR binds to CPD lesion with binding constant of $K_S=10^{-9}$, while it binds to undamaged DNA with a binding constant of $K_{NS}=10^{-5}$ [58]. Having almost 7.5 x 10^4 higher affinity to damaged DNA enables the enzyme to seek lesions on DNA duplex and efficiently disassociate after the repair process.

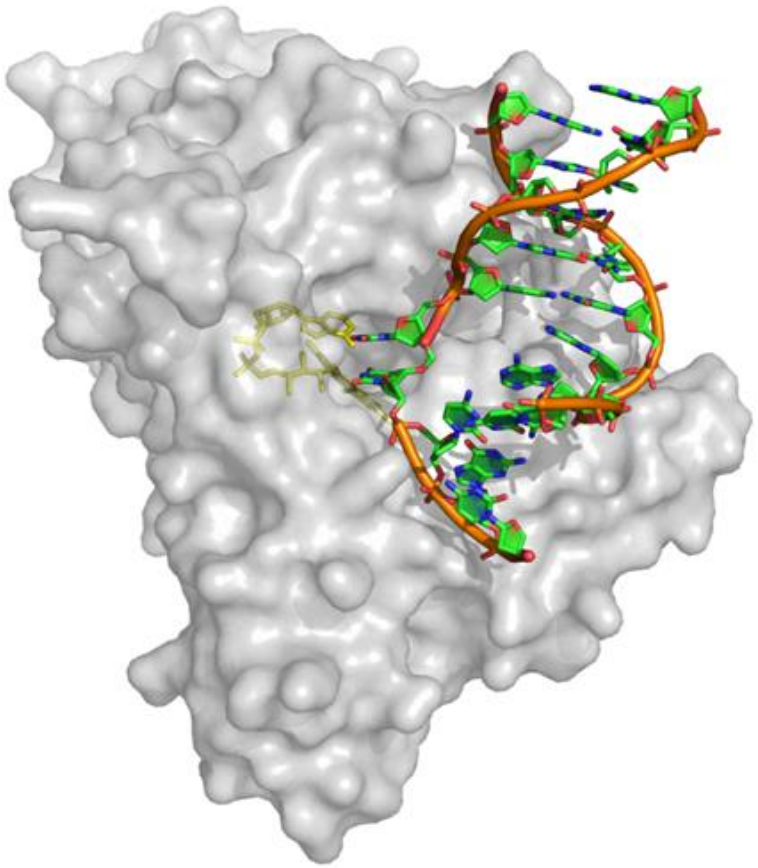

Figure 9. DNA-protein complex. Crystal structure of A. nidulans CPD PHR complexed with CPD photolesion (PDB ID: 1TEZ) [29]. *FAD cofactor is shown in yellow.*

In the first light-dependent process, photoinitiation, secondary chromophore acts as absorption enhancing pigment and absorbs blue light photons to transfer the light energy to catalytic cofactor. Photoreduction is the second process, enzymatically inactive neutral semiquinone $FADH^{\bullet}$ or oxidized FAD is *in vitro* reduced to enzymatically active anionic hydroquinone $FADH^{-}$. Since anionic hydroquinone is the physiological state of FAD, the second step may not be biologically relevant [28]. The third process, photorepair, involves the repair of the pyrimidine dimers by $FADH^{\bullet}$.

Photorepair of CPD photoproducts involves six well-defined elementary steps: three electron transfer, two bond-breaking and one bond making steps [59]. Figure 10 demonstrates the all resolved elementary steps for CPD repair. In these elementary steps, two competitions are observed. The first competition involves 250 ns forward electron transfer from excited $FADH^{-*}$ to CPD lesion and 1.3 ns excited $FADH^{-*}$ deactivation process. Splitting of C5-C5' bond occurs ultrafast in less than 10 ps. The second competition is the C6-C6' bond splitting with an average time 90 ps relative to futile back electron transfer with no repair in 2.4 ns. The electron returns in 700 ps to $FADH^{\bullet}$ from repaired lesion to restore active anionic hydroquinone state. The photocycle is completed without any net charge change in the redox state of $FADH^{-}$.

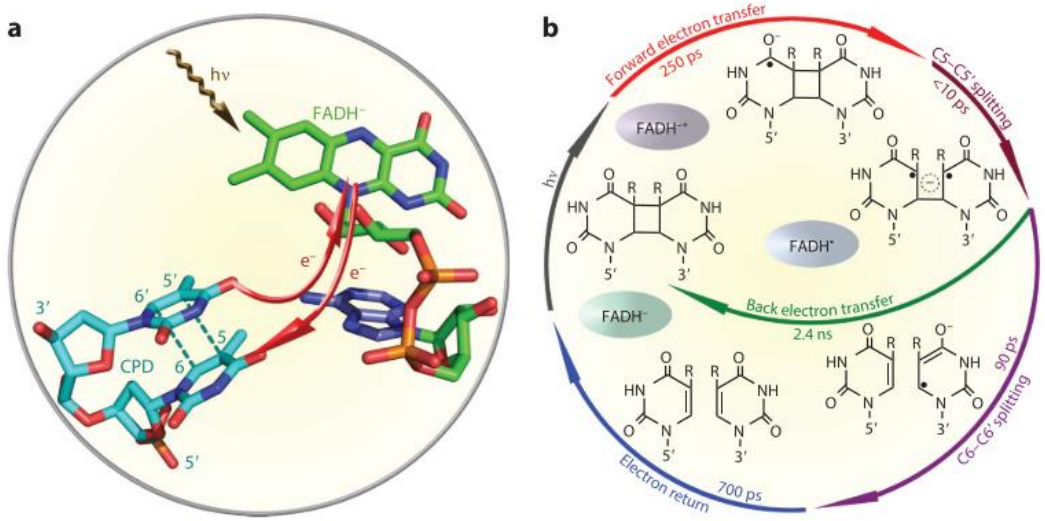

Figure 10. The reaction mechanism of CPD photolyases. (a) Relative position of FAD and CPD photoproduct. (b) Resolved elementary steps in the CPD repair by CPD photolyases. (Reproduced from the reference [5] *with permission of ANNUAL REVIEWS in the format Thesis/Dissertation via Copyright Clearance Center)*

Due to difficulties in substrate synthesis, instability of the enzymes and the complex repair mechanism, understanding (6-4) PHRs has been a challenging process [5]. In fact, ultrafast spectroscopy [60] and X-ray structure studies [61] identified a different mechanism than CPD repair (Figure 11) . Repair of 6-4PP involves a proton transfer from nearby histidine amino acid (H365 of *D. melanogaster* and H364 of *A. thaliana* (6-4) PHR) to the lesion after initial ET. Overall, with 0.8 stretched parameter, electron is transferred from excited $FAHD^{-*}$ to 5' side of DNA in 225 ps. Then a competition involves between the futile back electron transfer to $FADH^{\bullet}$ without repair in 50 ps (branching 0.9), and proton transfer from histidine residue in 425 ps (branching 0.1). Catalytic proton transfer is the key step for repair and determines the repair efficiency. Although, reaction mechanism and the intermediates after proton transfer is not well-defined, proton transfer initiates a series of atom arrangements to split C6-C4, and photocycle is completed with the return of proton and electron to histidine and $FAHD^{\bullet}$, respectively.

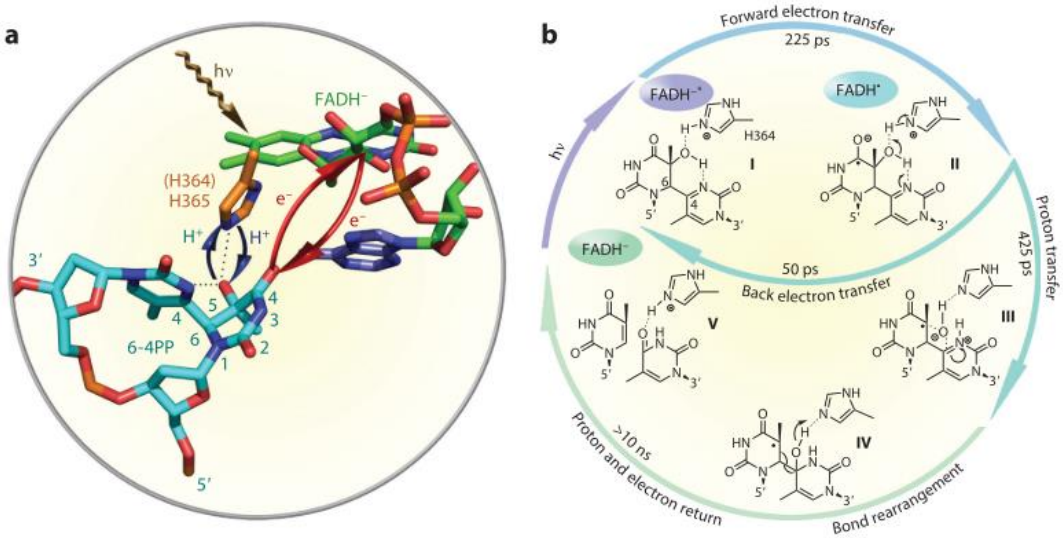

Figure 11. The reaction mechanism of (6-4) photolyases. (a) Relative position of FAD, (6-4)PP and histidine residue. (b) Repair of (6-4)PPs by (6-4) photolyases. (Reproduced from the reference [5] *with permission of ANNUAL REVIEWS in the format Thesis/Dissertation via Copyright Clearance Center)*

2.2.5 Classification of CPFs

Cryptochrome/photolyase family is a large family whose members are widely distributed in all three kingdoms of life. Classification of CPF members are achieved by combination of in silico approaches and biochemical assays [3]. CPF is functionally divided into two major classes: photolyases that can repair CPD or (6-4) photolesions, and cryptochromes that lost their DNA repair ability and gain diverse functions in circadian clock, transcription regulation, photoreception and magnetoreception pathways. Phylogenetically, CPF is divided into eleven classes: Class I, Class II, Class III PHRs; eukaryotic (6-4) PHRs; ssDNA PHRs (initially named as CRY-DASH); FeS-BCPs; plant CRYs, Type-1, Type-2, Type-3 CRYs; and sponge CRYs [3]. Often, the phylogenetic classification of CPF agrees with the functional characteristics of the class members. Class I, Class II and Class III PHRs are CPD photolyases. Class 0 PHRs were initially misclassified as CRY-DASHs; later, their repair activity on single-stranded DNA has been showed and today they are called ssDNA PHRs [8]. Eukaryotic (6-4) PHRs and FeS-BCP classes are photolyases with (6-4) PP specificity. Additionally, dual functionality of *R. sphaeroides* CryB has been proposed in both DNA repair and photoreception [62]. Based on their sequence similarities, cryptochromes are classified as animal CRYs (Type 1, Type 2, Type 4 CRYs) and plant CRYs. Plant CRYs, in general, function as photosensors. Humans have two cryptochromes (CRY1 and CRY2), both belonging to Type-2 CRYs. CRY1 and CRY2 function in the transcription-translation feedback loop that regulates the circadian rhythm [31]. Biochemical classification of CPF includes criteria such as protein function, substrate specificity and cofactor content. Despite functional similarities, Class I and Class III PHRs are structurally more related to Plant CRYs than Class II PHRs. Similarly, Eukaryotic (6-4) PHRs more closely related to animal cryptochromes than their prokaryotic counterparts (FeS-BCP).

2.3 Nucleotide Excision Repair

In the early 1960s, researches on the photoreactivation concept led the discovery of another major DNA repair mechanism: nucleotide excision repair (NER). The discovery of NER mechanism was a result of following observations on UV-resistant and UV-

sensitive *E. coli* strains [63][64]: When UV exposed *E. coli* cells kept under dark conditions and supplied with glucose as energy source, they were able to recover the damages of UV light [18]. In fact, this dark reactivation concept was not observed with UV-sensitive *E. coli* strain that carries a mutation in uvrA locus (AB18886). To understand the faith of thymine dimers during 'dark reactivation' process, cells were sonicated, and the supernatant was precipitated with trichloroacetic acid (TCA). TCA precipitates nucleic acid polymers longer than 20 nucleotides. In UV-resistant strain, thymine dimers were detected in TCA-soluble fraction while dimers were remained in TCA-insoluble fraction of UV-sensitive strain. These results suggested that, without a light source, cells were able to recover the damage by excising the lesion as short oligonucleotides; and a gene at uvrA locus might be functioning during this process. Further studies revealed all free-living organisms carry excision repair genes[65].

NER mechanism can be divided into 3 steps: damage recognition, excision, and gap filling. NER system recognizes helix-distorting, bulky DNA lesions and adducts on the genome [66]. Therefore, it can repair a wide range of structurally unrelated lesion such as CPDs, 6-4 PPs, cis-platin-d(GpG) diadduct and benzo(a) pyrene diolepox-ide [66][65]. According to the damage recognition site and mechanism, NER pathway is divided into two: Transcription-coupled repair (TCR) and global genomic repair (GGR). TCR pathway is initiated by the bulky lesions on transcribed part of the DNA, while GGR repairs the lesions on non-transcribed DNA.

Overall, bulky lesions on genomic DNA distorts the activity of RNA polymerase. In TCR, stalling of RNA polymerase initiates the NER system recruits the proteins functioning in incision process. In GGR, damage recognition is achieved by XPC together with RPA and XPA. Downstream excision and gap filling steps are conserved in both pathways (Figure 12). The lesion is excised from both 5' and 3' sides as short oligonucleotides (in human~30 nt in length, in *E. coli*~12nt in length) by dual incision. The gap is filled according to complementary strand by DNA polymerase and ligated by ligase.

Since placental mammals do not possess photolyase-mediated repair mechanism, UV induced damages are removed from genome mostly by NER. Defects in NER system leads to high UV-sensitivity and subsequently carcinogenic effects. For instance,

Xeroderma pigmentosum (XP) is an inherited disease caused by deficiencies in excision repair system. Symptoms of XP include severe sunburn, freckling and skin pigmentation after a few minutes of exposure to sunlight. XP patients have a 10,000 times higher non-melanocytic skin cancer risk [67].

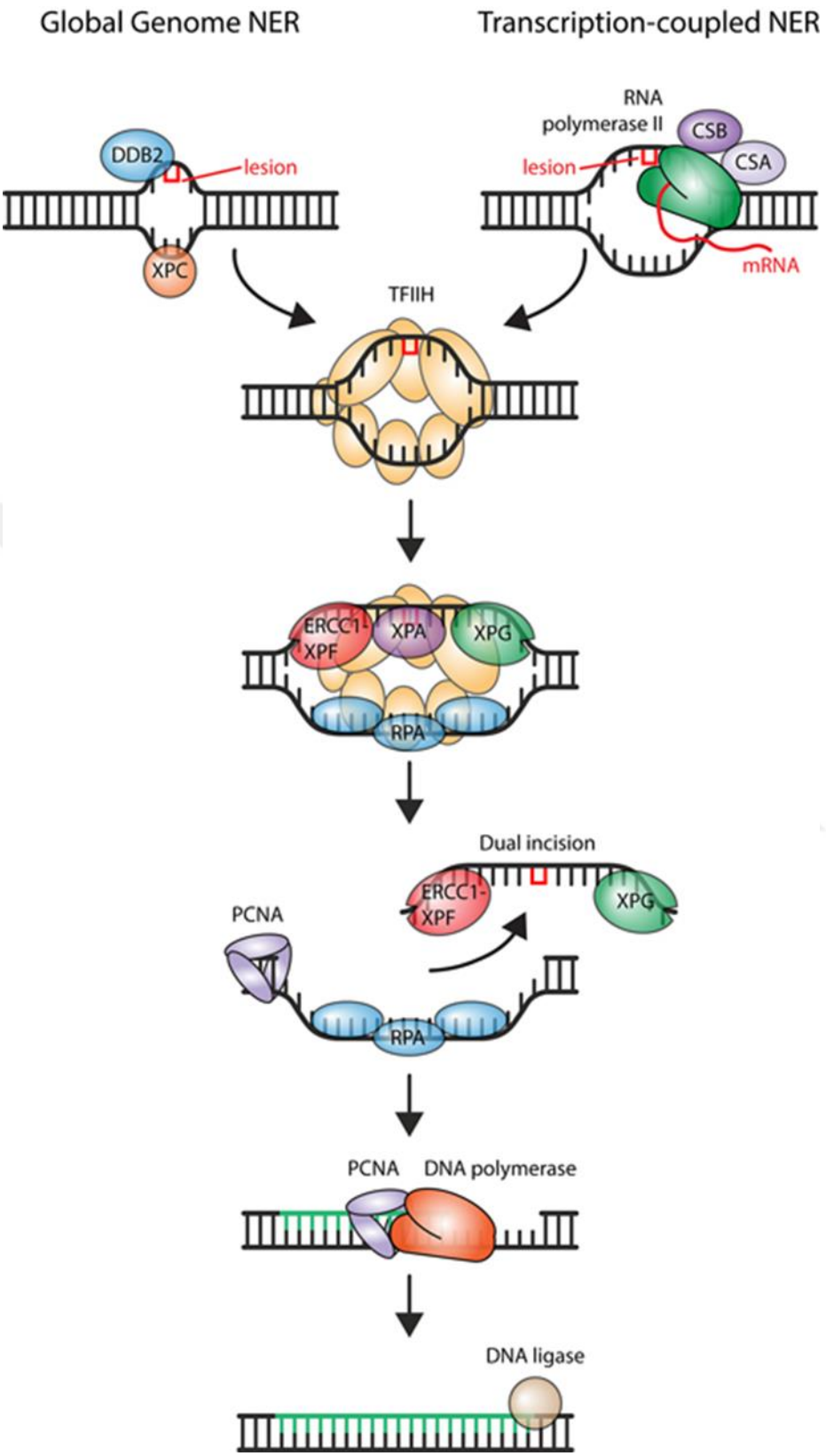

Figure 12. Mechanism of nucleotide excision repair in humans.

2.4 Vibrio cholerae: CPF members and Blue Light Response

Vibrio cholerae is gram-negative bacterium with flagellum whose habitat is aquatic ecosystems [68]. Some strains of *V. cholerae* are pathogenic secreting enterotoxins causing the disease, cholerae. The primary symptom of the disease is watery, severe diarrhea. Bacteria is transmitted to its host through fecal-oral route and colonizes in small intestine.

V. cholerae is an enteric bacterium and it is not exposed to light in its host. But, under its natural aquatic habitat, and during the transition to it host, UV light may introduce damages to its genomic DNA [69]. Therefore, *V. cholerae* should employ the mechanism that reverse such damages. In 2000, the complete genomics sequence of the *V. cholerae* was published [70]. *V. cholerae* genome contains two circular chromosomes consisting of 2,961,146 bp and 1,072,314 bp encoding 3885 open reading frames. Several genes are determined to encode proteins functioning in the DNA repair and DNA damage response pathways such as photoreactivation, nucleotide excision repair, mismatch-excision repair, base-excision repair, AP endonuclease etc.

Until this study, it was thought there are three *V. cholerae* genes belonging to cryptochrome/photolyase family: *VCA0057* encoding a CPD PHR: VcPhr, *VC1814* encoding a single-strand CPD PHR: VcCry1 and *VC1392* encoding another single-strand CPD PHR: VcCry2 [69][8]. In this study we introduced another member of cryptochrome/photolyase family *VCA0809* gene that encodes the first (6-4) PHR identified in *Vibrio cholerae*.

The effect of blue light on *V. cholerae* at transcriptome level was studied by RNA-sequencing [9]. The results suggested 6.3% of the Vibrio genome is regulated by blue light. CPF members are around 16 folds up-regulated under blue light, and this effect is diminished in ΔChrR ΔMerR double-knockout, light-blind mutant cells.

2.5 Aim of the Research

Aim of this research was to characterize a cryptochrome-photolyase family related protein in *Vibrio cholerae* O1 bivar Tor str. N16961. The gene, *Vca0809* encoding a putative CPF member took our attention after our RNA sequencing studies [9]. *VCA0809* gene is upregulated under blue light and has high homology to the CPF. The aim of this study was to identify the function of the protein and characterize its structure using biochemical and computational methods.

In 2003, Aziz Sancar and his team purified and characterized three members of CPF in *V. cholerae*: VcPhr, VcCry1 and VcCry2 [69]. VcPhr is a CPD photolyase; and VcCry1 and VcCry2 are single-strand specific CPD photolyases.

To investigate the function of the protein, gene of interest was cloned into an expression/purification vector, pMalc2x. Protein was overexpressed by IPTG and purified by affinity chromatography. UV-vis absorption and fluorescence characterizations were performed to investigate the cofactors in protein structure. To classify a protein as CRY of PHR, the first thing to check is the repair activity *in vitro*. Repair activity of purified Vc(6-4) FeS-BCP was examined via slot-blot DNA repair assay. Further structural characterization was performed by computational and spectroscopic methods.

Chapter 3:
MATERIAL METHODS

3.1 Bacterial Strains, Plasmids and Cloning:

For the expression of Vca0809 and VcPhr, E. coli strain UNC523F'lacI6 (phr::kan uvrA::Tn10) was used as the host strain. pMAL-c2x expression plasmid (New England, BioLabs) was used to express maltose binding protein (MBP) fused photolyases. Vca0809 was amplified by PCR with following primers: Forward-Vca0809-EcorI (5'ATTTCAGAATTCATGCGCTATTCCGTTGTGCGATTG), Reverse-Vca0809-PstI (5' GCTTGCCTGCAGTTATAAACTTTCAATCTGGCTCAGAT). PCR product was cloned upstream of malE gene from EcoR I and Pst I restriction sites. Sequences of the cloned genes were confirmed by sequencing of the inserts.

3.2 Generation of Vca0809 Null Mutant Vibrio cholerae

Vca0809 null mutants were generated as described previously [71]. Briefly,~500 bp from 5' region and ~500 bp from 3' region of the target gene was amplified by PCR. For 5' region amplification following primers were used:
Vca0809_Part1_XbaI_F1: 5'-AAC TCT AGA ATG CGC TAT TCC GTT GTG-3' (27mer),
Vca0809_Part1_R1: 5'-CTG CGC TCC TAA ATG ATT GCG TGC TTC AGG TTT GCC ATC AGC CGT C-3' (46mer).
For 3' region amplification following primers were used:
Vca0809_Part2_F2:5'-GAC GGC TGA TGG CAA ACC TGA AGC ACG CAA TCA TTT AGG AGC GCA G-3' (46mer),
Vca0809_Part2_SacI_R2: 5'-TAT GAG CTC TTA TAA ACT TTC AAT CTG-3' (27mer)
Two amplified regions were combined to construct a deletion fragment by splicing by overlap extension PCR. Combined DNA fragments, lacking a major part of coding sequence, was cloned into pGP704-sacB28 suicide vector from XbaI and SacI restriction sites. A conjugative *E. coli* SM10λpir strain was used to host pGP704-sacB28 deletion plasmid. Biparental mating was performed between WT *Vibrio*

cholerae and SM10λpir carrying deletion vector. Transconjugants were subsequently subjected to ampicillin and sucrose selections as described by the reference [72]. Double recombination yielded ampicillin resistant, sucrose sensitive strains that lack a major part of coding sequence. Deletion of the target genes were confirmed by PCR with following primers:
Vca0809-Flank-Forward: 5' TTA AAT AAC TAA TAT CTT CATG and
Vca0809-Flank-Reverse-5' TAA CCT GTA ACC AAC AAA AATG.

3.3 Recombinant Protein Purification

For the purification of MBP fused Vca0809 and VcPhr proteins, Vca0809-pMALc2x and VcPhr-pMALc2x plasmids were transformed into *E. coli* UNC523 by heat shock. Purification was performed as described in pMAL Protein Fusion and Purification System Manual (New England, BioLabs). Briefly, transformed E. coli UNC523 cells were grown in 6 L of Luria-Bertani (LB) medium containing ampicillin (100 µg/mL) at 37 °C until A600 value reaches 0.5. To induce expression of the fusion protein, isopropyl β-D-1-thiogalactopyranoside (IPTG) was added to a final concentration of 0.3 mM and cultures were incubated at 22°C for 24 hours. Cells were harvested by centrifugation and resuspended in the column buffer containing 20mM Tris-HCl pH 7.4, 200mM NaCl and 1mM EDTA. Cell lysis was performed by 20 min incubation with lysozyme (200 µl/ml) followed by sonication for 3 minutues with 0.5 sec strikes and 0.5 sec intervals using a sonicator at 40% amplitude (Branson Ultrasonics). Cell debris was removed by ultracentrifugation at 15000 xg for 45 min; and cell free extract was transferred onto the 15 ml amylose resin column. After extensive washing with the column buffer, fusion protein was eluted with column buffer containing 10 mM maltose. SDS-PAGE followed by a Coomassie staining was performed to determine fractions containing fusion protein.

Spectroscopic analysis was performed in the elution buffer immediately after purification. Purified MBP-fused photolyases were dialyzed in storage buffer containing 50 mM Tris-HCl, 100 mM NaCl, 1 mM EDTA, 5 mM dithiothreitol, and 50% (v/v) glycerol, and stored at -20°C.

3.4 Spectroscopic Analysis

The absorption and fluorescence spectra of freshly purified fusion protein were recorded with UV-1700 Spectrophotometer (Shimadzu) and Spectrofluorometer FS5 (Edinburgh Instruments), respectively. Absorption spectrum between 240 nm and 750 nm was recorded in a quartz cuvette. Fluorescence spectra was recorded with excitation wavelength between 300 nm – 470 nm excitation and 400 nm – 550 nm emission wavelengths.

To determine the released cofactors, the native protein was denatured by heating at 95 °C for 10 min, in elution buffer containing 0.8% SDS and 0.1 M HCl. Denatured apoenzyme was removed by centrifugation and absorption spectrum of released cofactors were recorded by spectrophotometer.

3.5 RNA isolation and qRT-PCR

Blue light and qRT-PCR experiments are performed as described by Tardu et al. [9]. Briefly, *V. cholerae* cells were overnight grown in LB medium at 37 ºC under dark conditions. Dark-grown cells were diluted (1:50) in LB and grown until OD600 reaches 0.8-1.0. Then, samples were washed and resuspended in PBS. Blue light experiments were conducted with a black light fluorescence source mainly emitting 365 nm. Half of the cells were kept under dark conditions, and the other half of the cells were exposed to BL with an intensity of 0.5 J m^{-2} s^{-1} for 45 minutes. After light experiment, cells were collected by centrifugation and their total RNA were extracted using TRIzol reagent (Invitrogen) according to manufacturer's manual. After DNase I treatment, cDNA was synthesized from 1 µg RNA using reverse transcriptase and random hexamers. qRT-PCR was performed with a master mix containing gene specific primers: Forward-Vca0809-RT: 5'GTACGTTCGCCATCACATTC, Reverse-Vca0809-RT: 5'AGATCCAGATGCCATACGTG. DNA amplification was measured by CFX Connect Real-Time System (BIO-RAD) with following program: 95 °C for 10 min; 40 cycles of 95 °C for 2 s, 56 °C for 10 s, and 72 °C for 10 s. *gapdh* gene (Forward-gapdh-RT: 5'GGTCAAGACATCGTTTCTAACGC, Reverse-gapdh-RT:

5’GTTGAAGATGGGATGATGTTTTG) is used as internal control and relative mRNA expression was calculated using CFX Manager 3.1 software (BIO-RAD).

3.6 Electroporation

In photoreactivation complementation assay, Δ*Vc(6-4) FeS-BCP* Vibrio cells were complemented with pMAL-c2x- Vc(6-4) FeS-BCP vector by a slightly modified version of the electroporation methods described by the references [73] [74]. Briefly, *V. cholerae* cells were grown in 30 ml LB medium to log phase (OD 600 = 0.5-0.7) and collected by centrifugation at 4000 g, 4 ºC. Cells were washed three times with 30 ml prechilled electroporation buffer containing, 408 mM sucrose, 7 mM Na_2HPO_4, 15% glycerol (pH = 6.6). The cell pellet was collected in 150 µl cold buffer and 50 µl cell suspension was mixed with 0.5 µg plasmid DNA. After 15 min incubation on ice, cell-DNA mixture was transfer to 0.2-cm gap electroporation cuvettes and exposed to electric field (2.5 kV, 1 pulse) by BioRad Micropulser. Electroporated cells were transferred into 450 µl antibiotic-free LB medium and incubated for 45 min at 37 ºC. Finally, the cells were spread onto LB-agar medium containing corresponding antibiotics.

3.7 Photoreactivation and Survival Curve

OSRAM germicidal lamp (G8T5/OF) and Sylvania black light lamps (F15T8/BLB) were used as 254 nm UV light and 365 nm blue light sources, respectively. Blue and UV light intensities were measured at 364 nm and 254 nm by UVX radiometer (Ultraviolet Products Inc). Photoreactivation experiments were performed as described by Worthington et al. [7]. Briefly, wild type *V. cholerae* and its mutant derivatives were overnight grown in LB medium at 37°C under dark conditions. Dilutions and washing steps were made in phosphate-buffered saline (PBS). Cells were collected by centrifugation, washed two times and 1:10 diluted. One-third of the cells were stored under complete darkness and defined as no-UV samples. Cells were exposed to UV light for 20, 40 and 80 seconds at a fluence rate of 0.5 J m^{-2} s^{-1} in a cell culture dish with constant stirring. After UV treatment half of UV exposed cells was kept in complete darkness and defined as dark samples; and the other half was used for photoreactivation.

Cover of the plates and a glass with 2 cm thickness were used to block UV light during photoreactivation experiments. Plates were treated with Sylvania F15T8/BLB black light for 90 min at a fluence rate of 2.5 J m^{-2} s^{-1}; photoreactivated cells were defined as Light samples. Light, dark and no-UV samples were diluted and spread on agar plates as triplicates. Dilutions were optimized to yield 15-150 colony forming units per plate. Plates were incubated overnight at 37 °C and colony forming units (CFU) were counted. Survival rates were calculated as follows: $Survival\ rate_{dark/light} = CFU_{dark/light} / CFU_{no\text{-}UV} * 100$. Photoreactivation experiments were performed under either complete darkness or dim yellow light to prevent uncontrolled photoreactivation.

3.8 DNA Slot Blot-based Repair Assay

pG5-luciferase vector was used as DNA substrate as describe in the reference [75]. To introduce pyrimidine dimers, 50 ng/µl pG5-luc vector was exposed to UV-C lamp (254 nm) with an intensity of 0.5 J/m2/s for 15 min. DNA samples were washed and concentrated to 1 µg/µl by sodium acetate followed by ethanol precipitation. DNA repair assay performed either by purified photolyases. Repair reaction was conducted with 1 µg substrate in 20 µl reaction buffer containing 20 mM Tris-HCl (pH 7.4), 100 mM NaCl, 10 mM DTT and 1 mM EDTA. Purified proteins at 2 µl volume were added to each reaction tube and incubated 20 minutes at room temperature to allow formation of enzyme-DNA complex. Light reaction was performed under 1 mW/cm^2 blue light (Sylvania F15T8/BLB) for 90 min with a 1 cm glass between the light source and the samples. After light reaction, samples were diluted in TE buffer and purified using NucleoSpin® Gel and PCR Clean-up (Macherey-Nagel). DNA was denatured by boiling at 100 °C for 10 min in a buffer containing 0.4 M NaOH and 10 mM EDTA. To neutralize the DNA, samples were immediately transferred to ice and supplemented with prechilled ammonium acetate (pH 7.0) to final concentration of 1 M. For (6-4)PP detection 1000 ng, and for CPD photoproduct detection 200 ng DNA samples were blotted to nitrocellulose membrane by Bio-Dot SF microfiltration apparatus (Bio-Rad) and washed with 2X saline-sodium citrate (SSC) buffer. The membrane was allowed to dry at 80 °C for 3 hours for the fixation. CPD and (6-4)PP UV damages were blotted by anti-CPD (Kamiya) and anti-(6-4)PP (Cosmo Bio) monoclonal antibodies which were

analyzed by an enhanced chemiluminescence reaction. ECL reaction was imaged with the ChemiDoc XRS Image Analyser (Bio-Rad).

3.9 Computational Structural Analysis

3.9.1 Sequence Alignment and Phylogenetic Tree Generation

Amino acid sequences of Cryptochrome/Photolyase family members were retrieved from NCBI and aligned by ClustalW [76]. Rooted phylogenetic tree with branch length was generated by Maximum Likelihood method and JTT matrix-based model in MEGA-X [77] [78]. The bootstrap consensus tree inferred from 500 replicates is taken to represent the evolutionary history of the taxa analyzed [79]. The tree with the maximum log-likelihood was presented with bootstrap values.

3.9.2 Homology Modelling

Sequences and crystal structures of CPF member were retrieved from NCBI and PDB, respectively. 3D Model structures were generated by Modeller [80]. RMSD values between two structures were calculated using backbone atoms (N, C alpha, C and O). Protein structures were analyzed and presented in PyMOL[81].

Chapter 4:
RESULTS AND DISCUSSION

4.1 Identification of the Vibrio cholerae (6-4) Photolyase

In our pervious study, we showed the effect of blue light at the transcriptomics level let us identified a gene highly up-regulated upon exposure to cells to blue light in *Vibrio cholerae* O1 bivar Tor str. N16961, which will be referred as *V. cholera* [9]. The gene (*VCA0809*) is located on the second chromosome and annotated as the "hypothetical protein VCA0809". During the annotation of this gene by Ancoript, it is suggested as a probable blue light photoreceptor. Therefore, we analyzed this gene against Cryptochrome/Photolyase (CPF) gene family. To elaborate that we first used 250 CPF genes to establish a molecular phylogenetic tree as described previously [4]. Results showed the *VCA0809* gene is grouped with (6-4) photolyases of iron-sulfur bacterial cryptochromes and photolyases (FeS-BCP) (Figure 13a). We then used ClustalW alignment tool to calculate degree of conservation between VCA0809 and other FeS-BCPs. Alignment analysis revealed that VCA0809 protein had 39.21% and 42.26 % sequence identity with *A.tumefaciens* PhrB and *R. sphaeroides* CryB, respectively (Figure 13b). These computational analysis suggested that *VCA0809* gene might be a probable (6-4) FeS-BCP, therefore we named this gene *Vc(6-4) FeS-BCP*.

A.

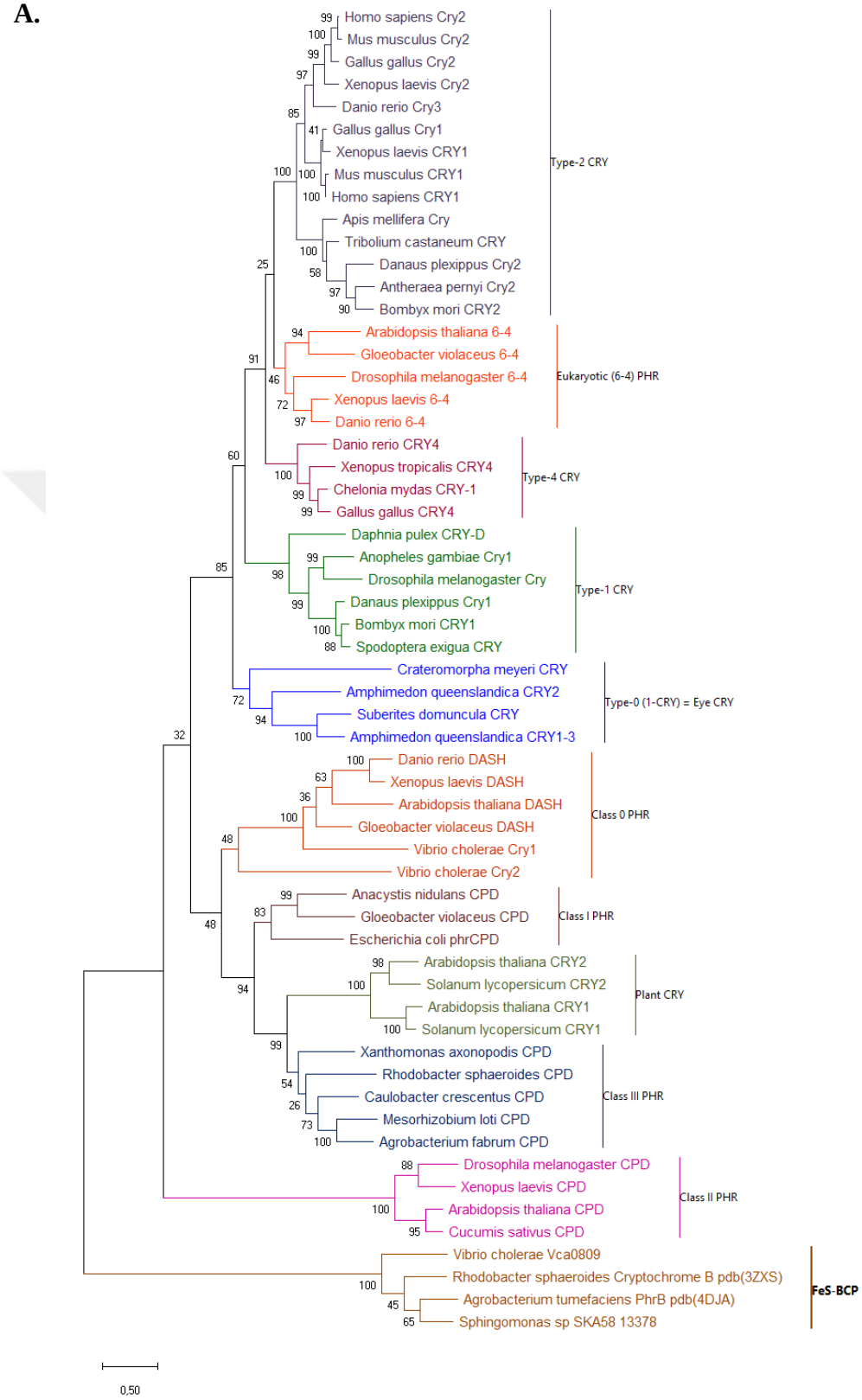
Homo sapiens Cry2
Mus musculus Cry2
Gallus gallus Cry2
Xenopus laevis Cry2
Danio rerio Cry3
Gallus gallus Cry1
Xenopus laevis CRY1
Mus musculus CRY1
Homo sapiens CRY1
Apis mellifera Cry
Tribolium castaneum CRY
Danaus plexippus Cry2
Antheraea pernyi Cry2
Bombyx mori CRY2
Type-2 CRY
Arabidopsis thaliana 6-4
Gloeobacter violaceus 6-4
Drosophila melanogaster 6-4
Xenopus laevis 6-4
Danio rerio 6-4
Eukaryotic (6-4) PHR
Danio rerio CRY4
Xenopus tropicalis CRY4
Chelonia mydas CRY-1
Gallus gallus CRY4
Type-4 CRY
Daphnia pulex CRY-D
Anopheles gambiae Cry1
Drosophila melanogaster Cry
Danaus plexippus Cry1
Bombyx mori CRY1
Spodoptera exigua CRY
Type-1 CRY
Crateromorpha meyeri CRY
Amphimedon queenslandica CRY2
Suberites domuncula CRY
Amphimedon queenslandica CRY1-3
Type-0 (1-CRY) = Eye CRY
Danio rerio DASH
Xenopus laevis DASH
Arabidopsis thaliana DASH
Gloeobacter violaceus DASH
Vibrio cholerae Cry1
Vibrio cholerae Cry2
Class 0 PHR
Anacystis nidulans CPD
Gloeobacter violaceus CPD
Escherichia coli phrCPD
Class I PHR
Arabidopsis thaliana CRY2
Solanum lycopersicum CRY2
Arabidopsis thaliana CRY1
Solanum lycopersicum CRY1
Plant CRY
Xanthomonas axonopodis CPD
Rhodobacter sphaeroides CPD
Caulobacter crescentus CPD
Mesorhizobium loti CPD
Agrobacterium fabrum CPD
Class III PHR
Drosophila melanogaster CPD
Xenopus laevis CPD
Arabidopsis thaliana CPD
Cucumis sativus CPD
Class II PHR
Vibrio cholerae Vca0809
Rhodobacter sphaeroides Cryptochrome B pdb(3ZXS)
Agrobacterium tumefaciens PhrB pdb(4DJA)
Sphingomonas sp SKA58 13378
FeS-BCP
0,50

B.

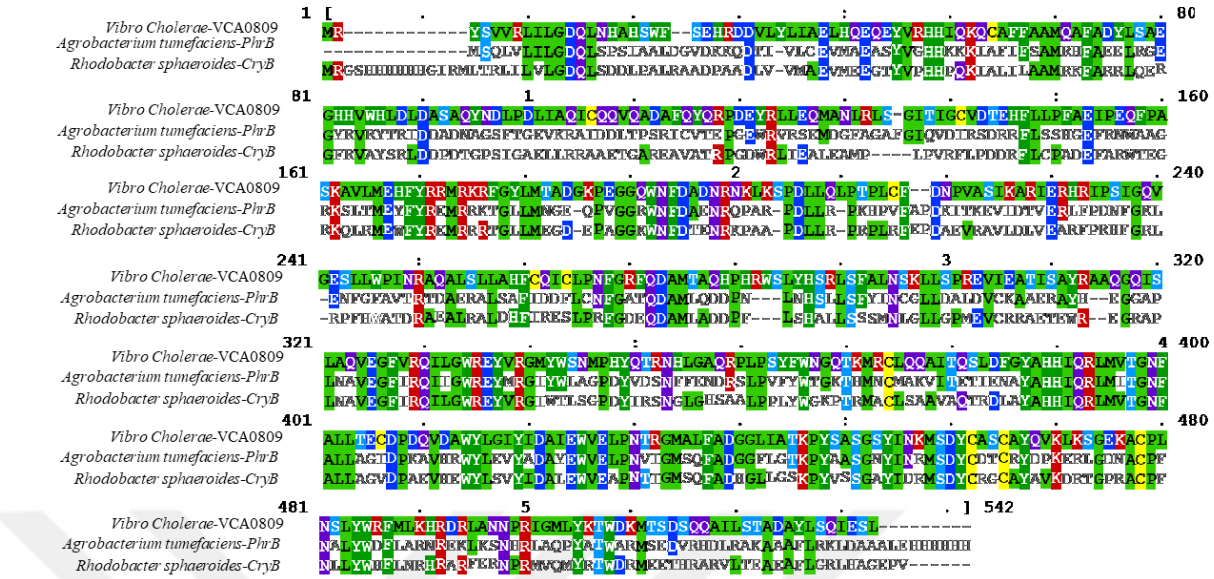

Figure 13. Sequence analysis of Vc(6-4) FeS-BCP. (a) Phylogenetic tree of Cryptochrome/Photolyase family generated by maximum likelihood method. (b) Sequence alignment of the Vc(6-4) FeS-BCP with A. tumefaciens PhrB and Rhodobacter sphaeroides CryB.

4.2 Expression and Purification of Vc(6-4) FeS-BCP and Spectroscopic Properties

Vc(6-4) FeS-BCP gene from *V. cholerae* cloned into the pMal-c2x where it was fused with MBP to promote the proper folding of the attached PHR and prevent aggregation [82]. Plasmid with PHR gene was transformed in *E. coli* UNC523 (phr::kan; uvrA::Tn10) for overexpression of Vc(6-4) FeS-BCP protein. After the sonication of the cells, crude extract was used for the purification of PL with amylose resin by affinity chromatography. The quality of the overexpression and purification was analyzed by SDS-PAGE followed by Coomassie blue staining (Figure 14a). After the purification, the dominant band was MBP- Vc(6-4) FeS-BCP with a molecular mass 110 kDa. As apparent from Figure 14a, the protein was >95% pure, exhibiting a brownish-yellow color (Figure 21) and appropriate for spectroscopic and enzymatic analyses.

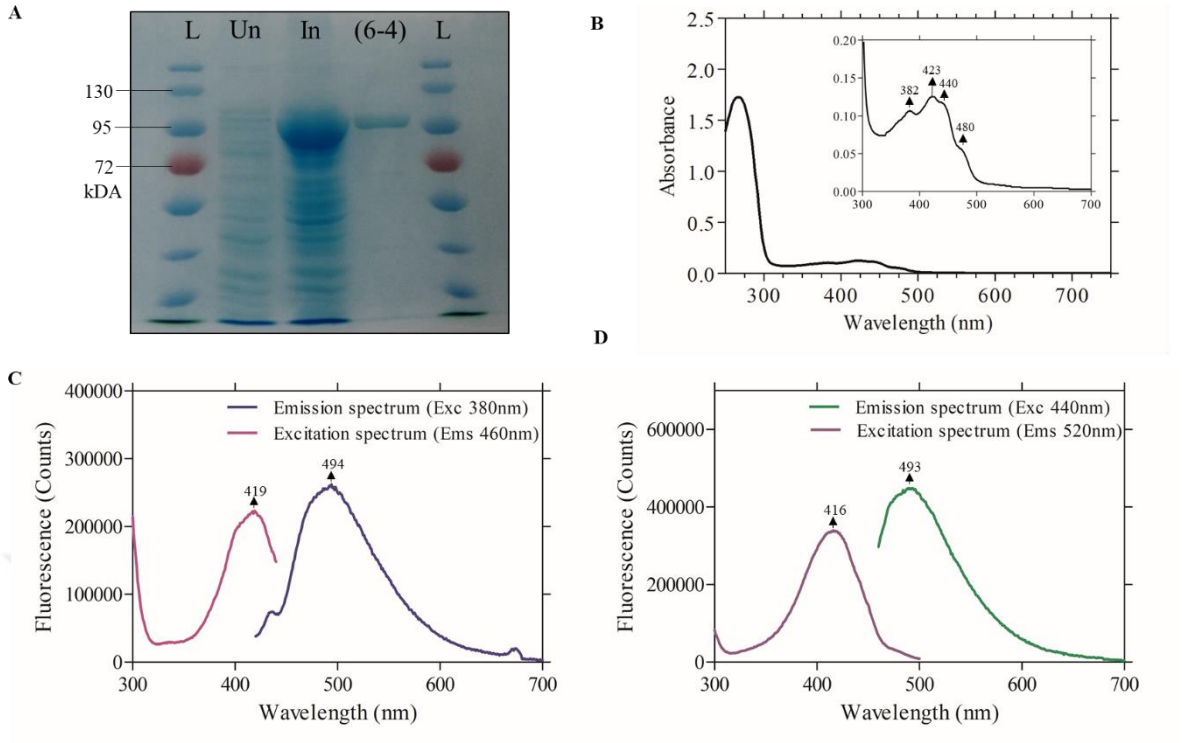

Figure 14. Purification of recombinant Vc(6-4) FeS-BCP protein and spectroscopic analysis. (a) Coomassie staining. Purified Vca0809 and CFE of E. coli expressing Vca0809 were separated by SDS-PAGE and visualized with Coomassie Blue. From left to right, L: Ladder, Un: Uninduced CFE, In: Induced CFE, (6-4) Vc(6-4) FeS-BCP-MBP fusion protein (b) Absorption spectra of Vc(6-4) FeS-BCP-MBP protein from 250 to 750 nm. Inset shows the expanded scale of the absorption spectrum from 300 to 700 nm. Fluorescence spectrum Vc(6-4) FeS-BCP-MBP with (c) folate and (d) flavin excitation emission wavelengths.

The FAD cofactor is necessary for the CPF protein family to perform their blue light-dependent functions [22]. The type second chromophore can vary depending on the type of organism, and can be methenyltetrahydrofolate (MTHF), 5-deazariboflavin, FAD, FMN or 6,7-dimethyl-8- ribityllumazine (DMRL) [2][22][11]. MTHF containing photolyases exhibit major absorption peaks at 375-410 nm. In addition, several peaks at 440 (exhibited by FAD_{ox}), 480, 580, and 625 nm (blue neutral radical form, $FADH^{\bullet}$) can be detected as the result of one- and two-electron oxidized species of FAD by absorption spectroscopy[83].

To analyze the chromophore content of the MBP-Vc(6-4) FeS-BCP, the purified MBP-Vc(6-4) FeS-BCP subjected to the absorption spectroscopy. MBP-Vc(6-4) FeS-BCP exhibited peaks at 382 nm, 423, 440 and 480 nm, and a tail extending up to 600 nm (Figure 14b). This result suggested that MBP-Vc(6-4) FeS-BCP possess DMRL (or MTHF) and a mixture of $FADH^{\bullet}$ and FAD_{ox}. To assess whether the peak we observed at

382 nm is DMRL, FAD or MTHF we performed florescence spectroscopy on the purified of MBP-Vc(6-4) FeS-BCP. Enzyme bound MTHF has a fluorescence emission maximum at 460-480 nm with an excitation maximum at 360-390 nm. Figure 14c shows the fluorescence spectra of MBP-Vc(6-4) FeS-BCP. When the excitation spectrum was measured for emission at 460 nm, an essentially symmetrical peak with λmax = 420 nm was obtained, consistent with DMRL being the predominant chromophore in near-UV in MBP-Vc(6-4) FeS-BCP as previously described [30]. If MTHF was the second chromophore, under this condition it was expected that λmax = 380 nm should be obtained as described for VcPhr [7]. Excitation at 380 nm gave a fluorescence spectrum with a single peak at 494 nm, consistent with the presence of both DMRL and FAD. Flavin has an emission maximum at 505-520 nm with excitation maxima at 370 nm and 440 nm. When the emission spectrum was recorded with 440 nm excitation wavelength, a peak at 493 nm was obtained, confirming the presence (Figure 14d). Under this condition, fluorescence emission of MBP-Vc(6-4) FeS-BCP was measured at 520 nm; a major excitation peak at 416 nm was observed, which coincides roughly with the absorbance maximum of DMRL; and, these results are consistent with a previous study for *A. tumefaciens* PhrB [30].

To further show the presence of DMRL, MBP-Vc(6-4) FeS-BCP was denatured by heating. After removal of denatured apoenzyme by centrifugation, the supernatant containing chromophores were subjected to absorption spectra and florescence spectroscopy. During the heating of the protein, MTHF is released from the protein, and 5-10 methenyl bridge that absorbs at 380 nm is broken to form 10-formyltetrahydrofolate which does not absorb near-UV region [7]. Therefore, if MBP-Vc(6-4) FeS-BCP possess only FAD or both FAD and MTHF, our expectation was that the absorption spectra of the released cofactors in the 300-600 nm range yields typical flavin absorption. In fact, the cofactors released from heat-denatured protein exhibited DMRL-FAD mixture absorption peaks at~380, 420 and 480 nm (Figure 15a), which is consistent with a previous study on *R. sphaeroides* CryB [84]. We, then, used fluorescence spectroscopy by measuring fluorescence emission at 520 nm, the approximate emission maximum of FAD, the maximum of the excitation spectrum was at 417 nm (Figure 15b), which coincides with DMRL absorption maximum. These

results confirmed that MBP-Vc(6-4) FeS-BCP possess FAD catalytic cofactor and DMRL as a secondary chromophore.

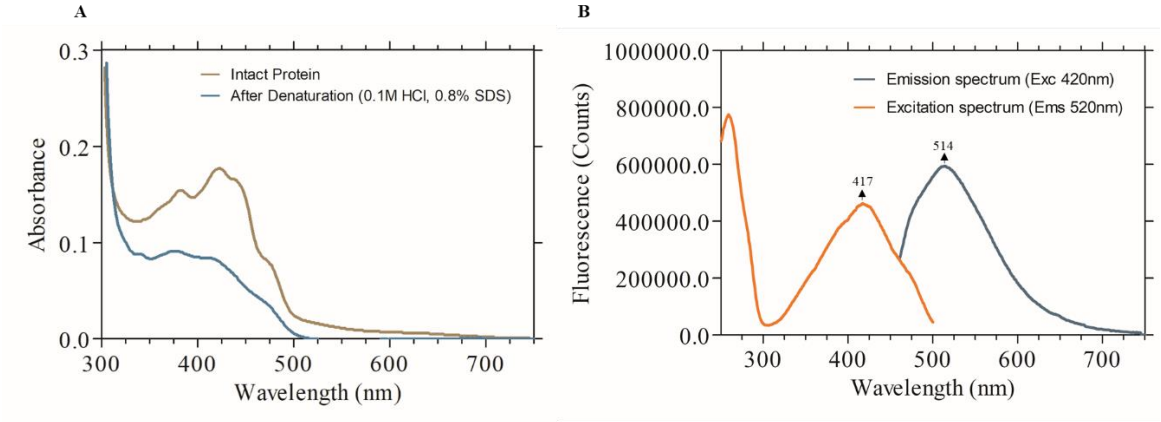

Figure 15. Released cofactors. (a) Absorption spectrum of released cofactors after heat denaturation in a solution containing 0.1M HCl and 0.8% SDS. (b) Fluorescence spectrum of released cofactors. Emission spectrum was recorded with 420 nm excitation wavelength and excitation spectrum was recorded with 520 nm emission wavelength.

4.3 Photoreactivation and Photolyase Complementation Assay

To determine the contribution of the Vc(6-4) FeS-BCP to biological photoreactivation, a sensitive complementation assay was performed. We first generated mutant strain of the *V. cholerae* in which *VCA0809* (strain designated as Δ*Vc(6-4) FeS-BCP)* was knock out as described previously [85]. *V. cholerae VcPhr::kan* mutant (designated as ΔVcPhr) lacking CPD PHR was used as a control as previously generated by insertional inactivation [7]. Cells were first exposed to 254-nm UV light at different doses. Half of the cells were kept under complete darkness and the other half was treated with photoreactivating light using a blue/black fluorescence lamp (366 nm). Then, each strain was plated onto LB-agar medium and overnight grown at 37 ºC. Colony forming units were counted to investigate photoreactivation rate. Expectedly, the wild type *V. cholerae* and mutant strains exposed to different doses of the UV-light exhibited dose dependent killing under dark conditions. When the samples were exposed to blue light, photoreactivation drastically eliminated the lethal photolesions and result in 670-fold (for 40 J/m^2 UV dose) survival in WT cells (Figure 16). On the other hand, ΔVcPhr cells result in only 5-6-fold survivors upon exposure to the blue light. After UV light exposure, ΔVc(6-4) FeS-BCP and wild type cells had similar killing rate, but ΔVc(6-4) FeS-BCP cells exhibited only 100-fold photoreactivation. To

further show that *Vc(6-4) FeS-BCP* gene contributes to DNA repair and photoreactivation, ΔVc(6-4) FeS-BCP cells were complemented with pMALc2x-Vc(6-4) FeS-BCP. Complemented cells that contain pMALc2x-Vc(6-4) FeS-BCP plasmid result in 1600 fold survivors upon exposure to the blue-light. Photolyase complementation assay indicated that pMALc2x FeS-BCP plasmid construct rescued irradiated (6-4) FeS-BCP deficient *V. cholerae* cells when compared to WT cells upon exposure to the blue light.

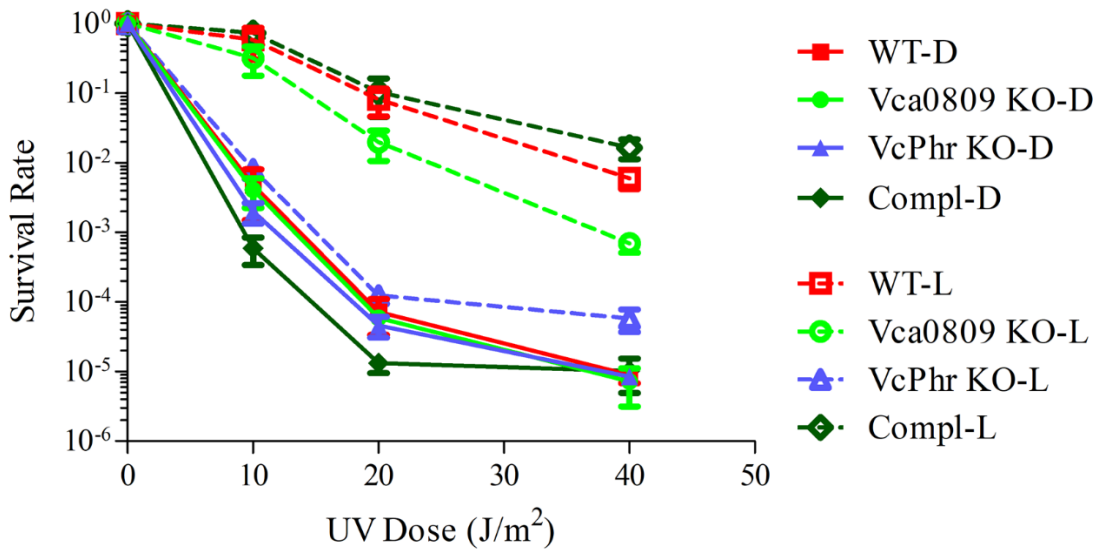

Figure 16. Photoreactivation and complementation assay. in vivo effect of Vc(6-4) FeS-BCP on the photoreactivation of Vibrio cholerae cells was investigated. Cells were initially exposed to UV-light and either kept under complete darkness or treated with photoreactivating light. CFU were counted to calculate survival rate of each strain. Straight lines indicate the dark kept cells and dashed lines indicate blue light treated cells. WT: Wild type, Vca0809 KO: ΔVc(6-4) FeS-BCP, VcPhr KO: ΔVcPhr, Compl: ΔVc(6-4) FeS-BCP cells complemented with pMALc2x-Vc(6-4) FeS-BCP.

4.4 DNA Slot-Blot Repair Assay

We next determined the activity of Vc(6-4) FeS-BCP by a DNA slot blot repair assay. In this assay, plasmids were exposed to UV light to introduce pyrimidine dimers and used as DNA substrate throughout the experiment. UV-exposed substrates were incubated with different amounts of purified Vc(6-4) FeS-BCP along with controls of CcPhr and Dm(6-4) photolyases. Samples were either treated with blue light for 90 min or kept under complete darkness. After cleaning, DNA substrates from each sample were denatured and fixed to nitrocellulose membrane. The amount of the unrepaired

DNA was assessed by monoclonal antibody that recognizes CPD or 6-4 photoproducts (Figure 17, top panel). For loading control, DNA fixed onto the membrane was analyzed by SYBR-gold staining, and the amount of DNA for each condition was determined as the same (Figure 17, lower panel). As expected, CcPhr and DmPhr had CDP and 6-4 repair activities, respectively. Vc(6-4) FeS-BCP had only blue-light dependent 6-4 activity. All these results suggested that Vc(6-4) FeS-BCP is a bacterial (6-4) photolyase.

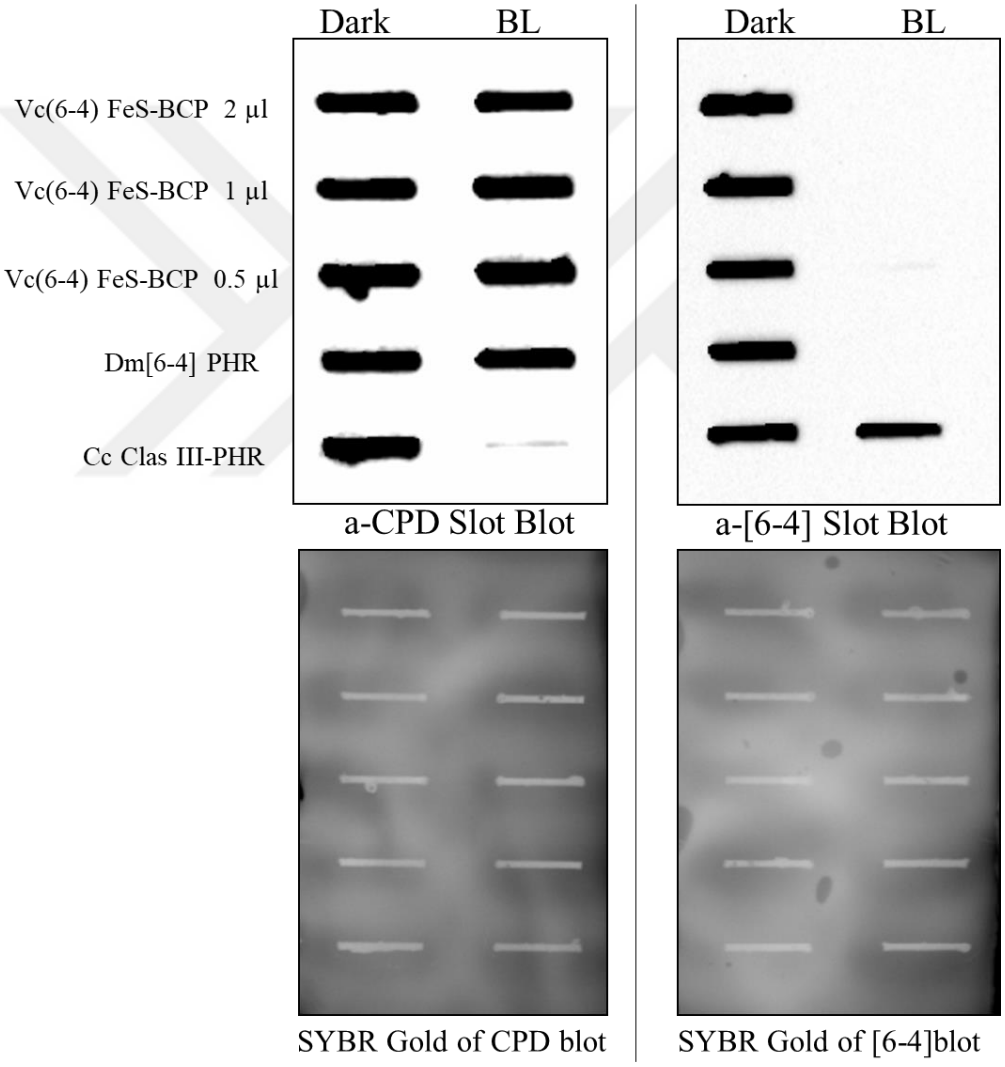

Figure 17. In vitro DNA repair assay. Immunoslot blot method was used to detect (a) unrepaired CPD and (b) (6-4) PP damages by using damage specific monoclonal antibodies. UV-treated plasmid DNA was incubated with corresponding purified proteins either under blue light or in complete darkness. DNA samples were loaded onto nitrocellulose and unrepaired DNA was detected by anti-CPD and anti-(6-4) antibodies. Left top panel corresponds to CPD blot and right top panel corresponds to (6-4) blot. DNA amounts loaded to each well were detected by SYBR-Gold staining and presented in lower panel.

4.5 Homology Modelling of Vc(6-4) FeS-BCP

Several crystal structure of Photolyase/Cryptochrome family members are available [2]. We homology modelled the Vc(6-4) FeS-BCP using crystal structures of photolyases: PhrB of *Agrobacterium.tumefaciens* [11], CryB of *Rhodobacter sphaeroides* [10], CPD photolyase of *E. coli* [32], and (6-4) photolyase of *Arabidopsis thaliana* [86]. The root mean square deviation (RMSD) was calculated between Vc(6-4) FeS-BCP and other structures (Table 1).

Table 1. RMSD values for model structures generated by homology modelling. Deviation of model structures from their template crystal structures was calculated by using backbone atoms (N, C, and O) and represented in RMSD values.

Protein Name **PDB ID** - Model Name	*PhrB* *A. tumefaciens* **4DJA** - Model 1	CRY-B *R. sphaeroides* **3ZXS** - Model 2	CPD PHR *E. coli* **1DNP** - Model 3	6-4 PHR, *A. thaliana* **3FY4** - Model 4
RMSD	1.24 Å	2.22 Å	9.74 Å	11.50 Å
# of aligned residues for RMSD	493	475	233	204

The results indicated that modeled structure of Vc(6-4) FeS-BCP was very similar to structures of bacterial (6-4) photolyases, PhrB of *A. tumefaciens*, CryB of *R. sphaeroides* with an RMSD of 1.24 Å and 2.22 Å, respectively (Figure 18). Vc(6-4) FeS-BCP is least conserved with its eukaryotic counterpart, *A. thaliana* (6-4) PHR.

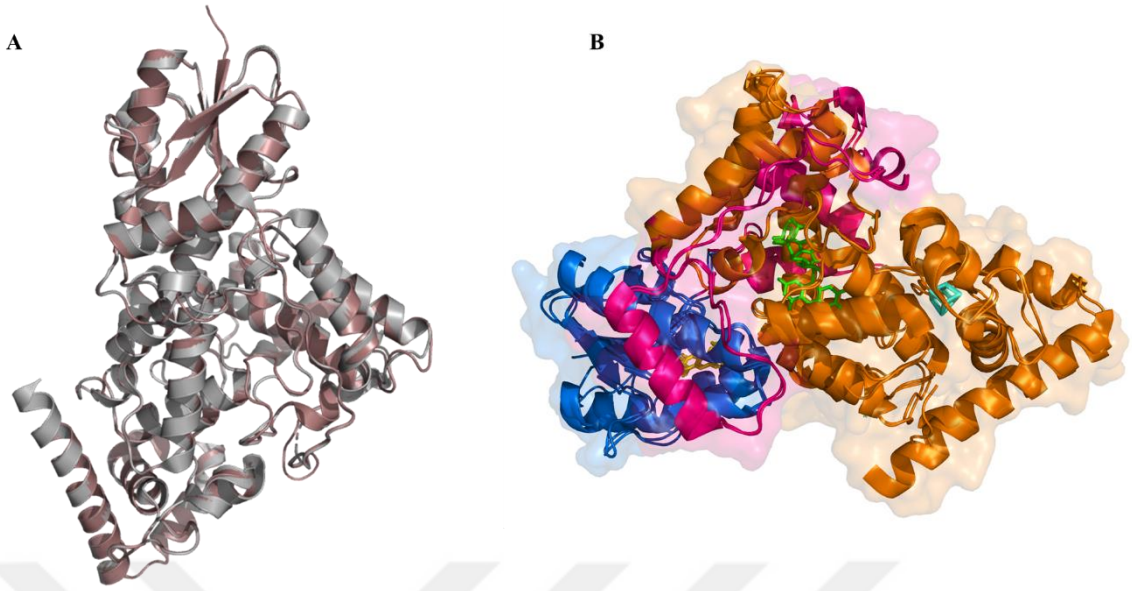

Figure 18. Predicted overall structure of Vc(6-4) FeS-BCP. (a) Ribbon representation of superimposed Vc(6-4) FeS-BCP (pink) and A. tumefaciens PhrB (white), PDB ID: 4DJA. (b) Superimposition of all prokaryotic (6-4) PHRs characterized up to date: V. cholerae Vc(6-4) FeS-BCP, A. tumefaciens PhrB (4DJA), R. sphaeroides CryB (3ZXS). [4Fe-4S] cluster(cyan), FAD (green) and DMRL (yellow) cofactors are adopted from PhrB. Photoantenna domain: blue, catalytic domain: orange, interdomain loop: pink.

We then analyzed the FAD binding site, [4Fe-4S] cluster, and DMRL binding site comparing with *A. tumefaciens* PhrB. As can be seen in Figure 19a, FAD interacting amino acids are well conserved in Vc(6-4) FeS-BCP and PhrB. Gln-313 (Glu-306 in PhrB), Met-417 (Met-410 in PhrB), Leu-377 (Leu-370 in PhrB) and His-373 (His-366 in PhrB) were conserved between Vc(6-4) FeS-BCP and PhrB. The crystal structure of the PhrB revealed that four Cys residues (Cys-350, Cys-438, Cys-441, Cys-454) are essential for coordination of [4Fe-4S] cluster [11]. We found these residues (Cys-357, Cys-445, Cys-448, Cys-461 of Vc(6-4) FeS-BCP) are also conserved in Vc(6-4) FeS-BCP (Figure 19b). Alignment of the Vc(6-4) FeS-BCP with other two amino acid sequences (Figure 13b) indicated that His365-His366-X-X-Arg369 motif (*A. tumefaciens* numbering), where the His366 homolog of eukaryotic (6-4) photolyases is essential for DNA repair [60], are well conserved. Finally, the amino acid residues interacting DMRL are also conserved between Vc(6-4) FeS-BCP and PhrB, except Phe-83 and Cys-32 of PhrB. Phe-83 is replaced with Leu-84 and Cys-32 is replaced with Ala-33 in Vc(6-4) FeS-BCP (Figure 19c).

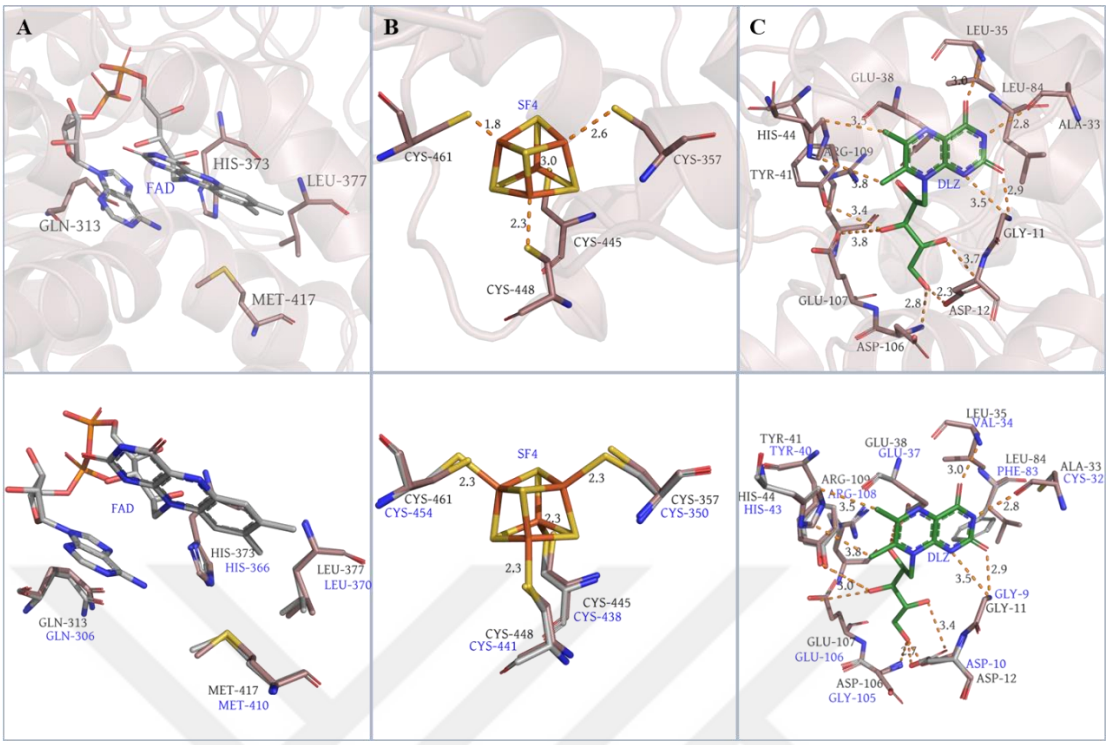

Figure 19. Cofactor arrangement in Vc(6-4) FeS-BCP. (a) FAD, (b) [4Fe-4S] cluster, (c) DMRL (DLZ) binding sites of model Vc(6-4) FeS-BCP are superimposed with the cofactors adopted from A. tumefaciens PhrB. Top panel: Model structure is represented in transparent ribbon diagram. Cofactors of PhrB and cofactor-interacting amino acids of Vc(6-4) FeS-BCP are represented in sticks. Lower panel: PhrB's cofactor-interacting amino acids (backbone carbons: white, residue labels: blue) and homologues amino acids in Vc(6-4) FeS-BCP (backbone carbons: pink, residue labels: black) are superimposed and represented in sticks.

4.6 Blue Light Regulation of Vc(6-4) FeS-BCP expression

Effect of the blue light on the expression of the *Vc(6-4)FeS-BCP* was determined by qRT-PCR as previously described. WT Vibrio cholerae cells were grown until OD_{600} reaches 0.8-1.0 under complete darkness. Then, cells were either exposed to blue light kept under dark condition. Total RNA of each sample was isolated, and cDNA was synthesized using reverse-transcriptase. qRT-PCR results suggested that *Vca0809* gene is upregulated 16-folds upon exposure to blue-light (Figure 20).

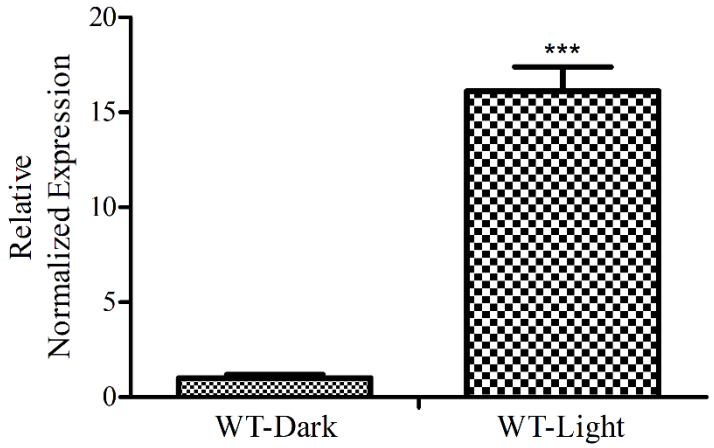

*Figure 20. qRT-PCR analysis of Vca0809 gene expression in WT Vibrio cholerae cells. Vibrio cholerae cells grown under dark conditions were either treated with blue light (WT-Light), or further kept under complete darkness (WT-Dark). Relative normalized expression of Vca0809 was calculated using gapdh gene as internal control. Experiment was repeated three times (n=3). Level of significance was calculated by two-way t-test (p***<0.001).*

Chapter 5:

CONCLUSION

In conclusion, we have identified and characterized the first (6-4) photolyase in *V. cholerae*. Gene *Vca0809* encodes an FeS-BCP protein named Vc(6-4) FeS-BCP that contains FAD catalytic cofactor, DMRL photoantenna and [4Fe-4S] cluster. *In vitro* repair activity was shown in a DNA Slot-Blot Repair assay; Vc(6-4) FeS-BCP specifically repair (6-4) PP under blue light condition. Homology modelling studies revealed that Vc(6-4) FeS-BCP is highly homologous to other members of FeS-BCP class members and the cofactor interacting amino acids are highly conserved in Vc(6-4) FeS-BCP, *A. tumefaciens* PhrB and *R. sphaeroides* CryB.

For a long time, (6-4) photolyases were thought to restricted to eukaryotic cells. Therefore, a little is known about prokaryotic (6-4) photolyases. There are future works to understand the molecular mechanism of FeS-BCPs in detail.

Chapter 6:
FUTURE DIRECTIONS

6.1 Energy transfer between DMRL and FAD of Vc(6-4) FeS-BCP

Photoantenna chromophores absorb blue light energy and transfer energy to catalytic cofactor via RET. Energy transfer between MTHF and $FADH^-$ was explained in detail in literature; but there is no direct study investigating the energy transfer from DMRL to $FADH^-$. It is known that DMRL lacking FeS-BCPs exhibit reduced DNA repair efficiency compared to wild-type protein. Therefore, understanding the energy transfer between Vc(6-4) FeS-BCP photoantenna chromophore and catalytic cofactor could be achieved by femtosecond fluorescence and transient absorption studies.

6.2 Functional characterization of [4Fe-4S] cluster

[4Fe-4S] clusters are known with redox potential and their contribution to electron transfer reactions. Additionally, [4Fe-4S] cluster is present in many DNA binding protein. Vc(6-4) FeS-BCP possess a [4Fe-4S] cluster in the catalytic alpha-domain which is mediated by four cysteine residues. Site-directed mutagenesis studies on PhrB revealed that mutations on one of these cysteine residues result in either not-expressed or non-soluble FeS-BCP protein. In fact, if [4Fe-4S] cluster is playing role in electron transfer, DNA binding or protein stability has not been concluded yet. Due to inability to purify [4Fe-4S] cluster lacking FeS-BCP proteins, computational methods such as molecular dynamics studies might give insights about the role of the [4Fe-4S] cluster in Vc(6-4) FeS-BCP.

6.3 Electron and proton transfer from $FADH^-$ to (6-4) PP

During the repair of (6-4) PPs, injection of electron is coupled with a proton transfer from a nearby histidine residue (H365 of *D. melanogaster* (6-4) PHR). This residue is also conversed in Vc(6-4) FeS-BCP (H373). Even though this phenomenon

suggests that prokaryotic (6-4) PHRs employs a similar mechanism with eukaryotic counterparts, experimental evidence is needed for further characterization.

6.4 *In vitro* photoreduction of oxidized FAD

Purification of photolyases in aerobic conditions may lead the oxidation of $FADH^-$ to FAD or $FADH^{\bullet}$. To restore functional redox state of FAD, photolyases can be photo-reduced under blue light via a highly conserved Trp-triad. FeS-BCP proteins lack the conventional Trp-triad, but different electron transfer paths can be proposed. Intraprotein electron transfer can be investigated by the combination of site-specific mutagenesis and femtosecond spectroscopy.

6.5 *Other functions of Vc(6-4) FeS-BCP*

R. sphaeroides CryB was initially described as cryptochrome due to its function in light- and singlet oxygen-dependent gene expression and its lack of DNA repair ability. Later, an evidence for (6-4) repair activity by CryB was presented. Dual characteristic of CryB and homology between Vc(6-4) FeS-BCP and CryB suggest that, Vc(6-4) FeS-BCP may also have dual-functioning properties: (6-4) PP repair and a cryptochrome-like function.

BIBLIOGRAPHY

[1] A. Sancar, “Structure and Function of DNA Photolyase and Cryptochrome Blue-Light Photoreceptors,” *Chem. Rev.*, 2003.

[2] I. H. Kavakli, N. Ozturk, and S. Gul, “DNA repair by photolyases,” in *Advances in Protein Chemistry and Structural Biology*, 1st ed., Elsevier Inc., 2019, pp. 1–19.

[3] N. Ozturk, “Phylogenetic and Functional Classification of the Photolyase/Cryptochrome Family,” *Photochem. Photobiol.*, vol. 93, no. 1, pp. 104–111, 2017.

[4] H. Asimgil and I. H. Kavakli, “Purification and characterization of five members of photolyase/cryptochrome family from Cyanidioschyzon merolae,” *Plant Sci.*, vol. 185–186, pp. 190–198, 2012.

[5] D. Zhong, “Electron Transfer Mechanisms of DNA Repair by Photolyase,” *Annu. Rev. Phys. Chem.*, vol. 66, no. 1, pp. 691–715, 2015.

[6] C. Saxena, H. Wang, I. H. Kavakli, A. Sancar, and D. Zhong, “Ultrafast dynamics of resonance energy transfer in cryptochrome,” *J. Am. Chem. Soc.*, 2005.

[7] E. N. Worthington, I. H. Kavakli, G. Berrocal-Tito, B. E. Bondo, and A. Sancar, “Purification and characterization of three members of the photolyase/cryptochrome family blue-light photoreceptors from vibrio cholerae,” *J. Biol. Chem.*, vol. 278, no. 40, pp. 39143–39154, 2003.

[8] C. P. Selby and A. Sancar, “A cryptochrome/photolyase class of enzymes with single-stranded DNA-specific photolyase activity,” *Proc. Natl. Acad. Sci.*, 2006.

[9] M. Tardu, S. Bulut, and I. H. Kavakli, “MerR and ChrR mediate blue light induced photo-oxidative stress response at the transcriptional level in Vibrio cholerae,” *Sci. Rep.*, vol. 7, no. December 2016, pp. 1–15, 2017.

[10] Y. Geisselbrecht, S. Frühwirth, C. Schroeder, A. J. Pierik, G. Klug, and L. O.

Essen, “CryB from Rhodobacter sphaeroides: A unique class of cryptochromes with new cofactors,” *EMBO Rep.*, vol. 13, no. 3, pp. 223–229, 2012.

[11] F. Zhang, P. Scheerer, I. Oberpichler, T. Lamparter, and N. Krauss, “Crystal structure of a prokaryotic (6-4) photolyase with an Fe-S cluster and a 6,7-dimethyl-8-ribityllumazine antenna chromophore,” *Proc. Natl. Acad. Sci.*, vol. 110, no. 18, pp. 7217–7222, 2013.

[12] A. Kelner, “Effect of Visible Light on the recovery of Streptomyces griseus Conidia from Ultra-Violet Irridation Injury,” *Proc. Natl. Acad. Sci.*, vol. 35, no. 2, pp. 73–79, 1949.

[13] C. S. Rupert, “Photoreactivation in Vitro of Ultraviolet Inactivated Hemophilus Influenzae Transforming Factor,” *J. Gen. Physiol.*, vol. 41, no. 3, pp. 451–471, 1958.

[14] J. Baker and S. Chaykin, “Isolation and Identification of the Irridation Product of Thymine,” vol. 41, pp. 548–550, 1960.

[15] D. L. Wulff and G. Fraenkel, “On the Nature of Thymine Photoproduct,” vol. 51, pp. 323–332, 1961.

[16] C. S. Rupert, “Photoenzymatic Repair of Ultraviolet Damage in DNA: I. Kinetics of the reaction,” *J. Gen. Physiol.*, vol. 45, no. 4, pp. 703–724, 1962.

[17] C. S. Rupert, “Photoenzymatic Repair of Ultraviolet Damage in DNA: II. Formation of an enzyme-substrate complex,” *J. Gen. Physiol.*, vol. 45, no. 4, pp. 725–741, 1962.

[18] A. Sancar, “Mechanisms of DNA Repair by Photolyase and Excision Nuclease (Nobel Lecture),” *Angew. Chemie Int. Ed.*, vol. 55, no. 30, pp. 8502–8527, 2016.

[19] H. Yokoyama and R. Mizutani, “Structural biology of DNA (6-4) photoproducts formed by ultraviolet radiation and interactions with their binding proteins,” *Int. J. Mol. Sci.*, vol. 15, no. 11, pp. 20321–20338, 2014.

[20] W. J. Schreier *et al.*, “Thymine dimerization in DNA model systems:

Cyclobutane photolesion is predominantly formed via the singlet channel," *J. Am. Chem. Soc.*, vol. 131, no. 14, pp. 5038–5039, 2009.

[21] K. Heil, D. Pearson, and T. Carell, "Chemical investigation of light induced DNA bipyrimidine damage and repair," *Chem. Soc. Rev.*, vol. 40, no. 8, pp. 4271–4278, 2011.

[22] A. Sancar, "Photolyase and cryptochrome blue-light photoreceptors," *Adv. Protein Chem.*, vol. 69, pp. 73–100, 2003.

[23] T. Douki, A. Reynaud-Angelin, J. Cadet, and E. Sage, "Bipyrimidine photoproducts rather than oxidative lesions are the main type of DNA damage involved in the genotoxic effect of solar UVA radiation," *Biochemistry*, vol. 42, no. 30, pp. 9221–9226, 2003.

[24] J. E. LeClerc, A. Borden, and C. W. Lawrence, "The thymine-thymine pyrimidine-pyrimidone(6-4) ultraviolet light photoproduct is highly mutagenic and specifically induces 3' thymine-to-cytosine transitions in Escherichia coli.," *Proc. Natl. Acad. Sci. U. S. A.*, vol. 88, 1991.

[25] J. Lee, G. Hwang, and B. Choi, "Solution structure of a DNA decamer duplex containing the stable 3′ T· G base pair of the pyrimidine (6–4) pyrimidone photoproduct : Implications for," *Proc. Natl. …*, vol. 96, no. June, pp. 6632–6636, 1999.

[26] L. O. Essen and T. Klar, "Light-driven DNA repair by photolyases," vol. 63, pp. 1266–1277, 2006.

[27] W. Harm, H. Harm, and C. S. Rupert, "Analysis of photoenzymatic repair of UV lesions in DNA by single light flashes. II. In vivo studies with Escherichia coli cells and bacteriophage," *Mutat. Res. - Fundam. Mol. Mech. Mutagen.*, vol. 6, no. 3, pp. 371–385, 1968.

[28] I. H. Kavakli and A. Sancar, "Analysis of the role of intraprotein electron transfer in photoreactivation by DNA photolyase in vivo," *Biochemistry*, vol. 43, no. 48, pp. 15103–15110, 2004.

[29] A. Mees *et al.*, “Crystal structure of a photolyase bound to a CPD-like DNA lesion,” no. December, pp. 1789–1794, 2004.

[30] F. Zhang *et al.*, “Crystal Structures of Bacterial (6-4) Photolyase Mutants with Impaired DNA Repair Activity,” *Photochem. Photobiol.*, vol. 93, no. 1, pp. 304–314, 2017.

[31] A. Sancar, “ Structure and Function of Photolyase and in Vivo Enzymology: 50th Anniversary ,” *J. Biol. Chem.*, vol. 283, no. 47, pp. 32153–32157, 2008.

[32] H. W. Park, S. T. Kim, A. Sancar, and J. Deisenhofer, “Crystal structure of DNA photolyase from Escherichia coli,” *Science (80-.).*, vol. 268, no. 5219, pp. 1866–1872, 1995.

[33] T. Todo *et al.*, “A new photoreactivating enzyme that specifically repairs ultraviolet light-induced (6-4) photoproducts,” *Nature*, vol. 361, pp. 371–374, 1993.

[34] M. Kai, T. Takahashi, T. Todo, and K. Sakaguchi, “Novel DNA binding proteins highly specific to UV-damaged DNA sequences from embryos of Drosophila melanogaster,” *Nucleic Acids Res.*, vol. 23, no. 14, pp. 2600–2607, 1995.

[35] I. Oberpichler *et al.*, “A photolyase-like protein from agrobacterium tumefaciens with an iron-sulfur cluster,” *PLoS One*, vol. 6, no. 10, pp. 2–11, 2011.

[36] M. G. Rossmann, D. Moras, and K. W. Olsen, “Chemical and biological evolution of a nucleotide-binding protein,” *Nature*, 1974.

[37] Z. Liu *et al.*, “Dynamic determination of the functional state in photolyase and the implication for cryptochrome,” *Proc. Natl. Acad. Sci.*, vol. 110, no. 32, pp. 12972–12977, 2013.

[38] H. Komori *et al.*, “Crystal structure of thermostable DNA photolyase: Pyrimidine-dimer recognition mechanism,” *Proc. Natl. Acad. Sci.*, 2001.

[39] B. Liu, H. Liu, D. Zhong, and C. Lin, “Searching for a photocycle of the cryptochrome photoreceptors,” *Current Opinion in Plant Biology*. 2010.

[40] M. Zhang, L. Wang, and D. Zhong, “Photolyase: Dynamics and Mechanisms of Repair of Sun-Induced DNA Damage.,” *Photochem. Photobiol.*, vol. 93, no. 1, pp. 78–92, 2017.

[41] C. Tan *et al.*, “Direct determination of resonance energy transfer in photolyase: Structural alignment for the functional state,” *J. Phys. Chem. A*, vol. 118, no. 45, pp. 10522–10530, 2014.

[42] C. Aubert, M. H. Vos, P. Mathis, A. P. M. Eker, and K. Brettel, “Intraprotein radical transfer during photoactivation of DNA photolyase,” *Nature*, 2000.

[43] Z. Liu *et al.*, “Determining complete electron flow in the cofactor photoreduction of oxidized photolyase,” *Proc. Natl. Acad. Sci.*, 2013.

[44] Z. Liu, C. Tan, X. Guo, J. Li, L. Wang, and D. Zhong, “Dynamic determination of active-site reactivity in semiquinone photolyase by the cofactor photoreduction,” *J. Phys. Chem. Lett.*, 2014.

[45] M. Byrdin, A. P. M. Eker, M. H. Vos, and K. Brettel, “Dissection of the triple tryptophan electron transfer chain in Escherichia coli DNA photolyase: Trp382 is the primary donor in photoactivation,” *Proc. Natl. Acad. Sci.*, 2003.

[46] Y. F. Li, A. Sancar, and P. F. Heelis, “Active Site of DNA Photolyase: Tryptophan-306 Is the Intrinsic Hydrogen Atom Donor Essential for Flavin Radical Photoreduction and DNA Repair in Vitro,” *Biochemistry*, 1991.

[47] S. T. Kim, A. Sancar, P. F. Heelis, T. Okamura, Y. Hirata, and N. Mataga, “Determination of Rates and Yields of Interchromophore (Folate → Flavin) Energy Transfer and Intermolecular (Flavin → DNA) Electron Transfer in Escherichia coli Photolyase by Time-Resolved Fluorescence and Absorption Spectroscopy,” *Biochemistry*, 1991.

[48] C. Saxena, A. Sancar, and D. Zhong, “Femtosecond dynamics of DNA photolyase: Energy transfer of antenna initiation and electron transfer of cofactor reduction,” *J. Phys. Chem. B*, vol. 108, no. 46, pp. 18026–18033, 2004.

[49] N. Öztürk *et al.*, “Purification and characterization of a type III photolyase from

Caulobacter crescentus," *Biochemistry,* 2008.

[50] T. Ueda, A. Kato, S. Kuramitsu, H. Terasawa, and I. Shimada, "Identification and characterization of a second chromophore of DNA photolyase from Thermus thermophilus HB27," *J. Biol. Chem.,* 2005.

[51] M. Fujihashi *et al.*, "Crystal Structure of Archaeal Photolyase from Sulfolobus tokodaii with Two FAD Molecules: Implication of a Novel Light-harvesting Cofactor," *J. Mol. Biol.,* 2007.

[52] C. P. Selby and A. Sancar, "The second chromophore in drosophila photolyase/cryptochrome family photoreceptors," *Biochemistry,* 2012.

[53] M. L. B. Magalhães, A. Argyrou, S. M. Cahill, and J. S. Blanchard, "Kinetic and mechanistic analysis of the Escherichia coli ribD-encoded bifunctional deaminase-reductase involved in riboflavin biosynthesis," *Biochemistry*, 2008.

[54] Y. Sato *et al.*, "Crystal structures of the lumazine protein from Photobacterium kishitanii in complexes with the authentic chromophore, 6,7-dimethyl-8-(1′-D-ribityl) lumazine, and its analogues, riboflavin and flavin mononucleotide, at high resolution," *J. Bacteriol.,* 2010.

[55] G. Payne and A. Sancar, "Absolute Action Spectrum of E-FADH2 and E-FADH2-MTHF Forms of Escherichia coli DNA Photolyase," *Biochemistry,* 1990.

[56] T. Tamada *et al.*, "Crystal structure of DNA photolyase from Anacystis nidulans," *Nat. Struct. Biol.,* 1997.

[57] I. Husain, G. B. Sancar, S. R. Holbrook, and A. Sancar, "Mechanism of damage recognition by Escherichia coli DNA photolyase.," *J. Biol. Chem.,* 1987.

[58] I. Husian and A. Sancar, "Binding of E. coli DNA photolyase to a defined substrate containing a single T< >T dimer," *Nucleic Acids Res.*, 1987.

[59] Z. Liu *et al.*, "Dynamics and mechanism of cyclobutane pyrimidine dimer repair by DNA photolyase," *Proc. Natl. Acad. Sci.,* vol. 108, no. 36, pp. 14831–14836,

2011.

[60] J. Li *et al.*, “Dynamics and mechanism of repair of ultraviolet-induced (6-4) photoproduct by photolyase,” *Nature*, 2010.

[61] M. J. Maul *et al.*, “Crystal structure and mechanism of a DNA (6-4) photolyase,” *Angew. Chemie - Int. Ed.*, 2008.

[62] A. von Zadow, E. Ignatz, R. Pokorny, L. O. Essen, and G. Klug, “Rhodobacter sphaeroides CryB is a bacterial cryptochrome with (6–4) photolyase activity,” *FEBS J.*, vol. 283, no. 23, pp. 4291–4309, 2016.

[63] R. P. BOYCE and P. HOWARD-FLANDERS, “RELEASE OF ULTRAVIOLET LIGHT-INDUCED THYMINE DIMERS FROM DNA IN E. COLI K-12.,” *Proc. Natl. Acad. Sci. U. S. A.*, 1964.

[64] R. B. Setlow and W. L. Carrier, “the Disappearance of Thymine Dimers From Dna: an Error-Correcting Mechanism,” *Proc. Natl. Acad. Sci.*, vol. 51, no. 2, pp. 226–231, 1964.

[65] J. T. Reardon and A. Sancar, “Nucleotide Excision Repair,” *Prog. Nucleic Acid Res. Mol. Biol.*, vol. 79, no. 04, pp. 183–235, 2005.

[66] G. Spivak, “Nucleotide excision repair in humans,” *DNA Repair*. 2015.

[67] J. O. Black, “Xeroderma Pigmentosum,” *Head Neck Pathol.*, vol. 10, no. 2, pp. 139–144, 2016.

[68] S. M. Faruque, M. J. Albert, and J. J. Mekalanos, “Epidemiology, genetics, and ecology of toxigenic Vibrio cholerae.,” *Microbiol. Mol. Biol. Rev.*, 1998.

[69] E. N. Worthington, I. H. Kavakli, G. Berrocal-Tito, B. E. Bondo, and A. Sancar, “Purification and characterization of three members of the photolyase/cryptochrome family blue-light photoreceptors from vibrio cholerae,” *J. Biol. Chem.*, 2003.

[70] C. M. Fraser *et al.*, “DNA sequence of both chromosomes of the cholera

pathogen *Vibrio cholerae*," *Nature*, vol. 406, no. 6795, pp. 477–483, 2000.

[71] C. Casper-Lindley and F. H. Yildiz, "VpsT Is A Transcriptional Regulator Required for Expression of vps Biosynthesis Genes and the Development of Rugose Colonial Morphology in Vibrio cholerae O1 El Tor," *J. Bacteriol.*, 2004.

[72] K. J. Fullner and J. J. Mekalanos, "Genetic characterization of a new type IV-A pilus gene cluster found in both classical and El Tor biotypes of Vibrio cholerae," *Infect. Immun.*, 1999.

[73] H. Marcus, J. M. Ketley, J. B. Kaper, and R. K. Holmes, "Effects of DNase production, plasmid size, and restriction barriers on transformation of Vibrio cholerae by electroporation and osmotic shock," *FEMS Microbiol. Lett.*, 1990.

[74] H. Hamashima, T. Nakano, S. Tamura, and T. Arai, "Genetic Transformation of Vibrio parahaemolyticus, Vibrio alginolyticus, and Vibrio cholerae Non O–1 with Plasmid DNA by Electroporation," *Microbiol. Immunol.*, 1990.

[75] J.-M. Park and T.-H. Kang, "DNA Slot Blot Repair Assay," *Bio-protocol*, vol. 5, no. 8, p. e1453, 2015.

[76] J. D. Thompson, D. G. Higgins, and T. J. Gibson, "CLUSTAL W: Improving the sensitivity of progressive multiple sequence alignment through sequence weighting, position-specific gap penalties and weight matrix choice," *Nucleic Acids Res.*, 1994.

[77] D. T. Jones, W. R. Taylor, and J. M. Thornton, "The rapid generation of mutation data matrices from protein sequences," *Bioinformatics*, 1992.

[78] S. Kumar, G. Stecher, M. Li, C. Knyaz, and K. Tamura, "MEGA X: Molecular evolutionary genetics analysis across computing platforms," *Mol. Biol. Evol.*, 2018.

[79] J. Felsenstein, "Confidence Limits on Phylogenies: An Approach Using the Bootstrap," *Evolution (N. Y).*, 1985.

[80] B. Webb and A. Sali, "Comparative protein structure modeling using

MODELLER," *Curr. Protoc. Bioinforma.*, 2016.

[81] Schrödinger, LLC, "The {PyMOL} Molecular Graphics System, Version~1.8," 2015.

[82] R. B. Kapust and D. S. Waugh, " Escherichia coli maltose-binding protein is uncommonly effective at promoting the solubility of polypeptides to which it is fused ," *Protein Sci.*, 1999.

[83] M. S. Jorns, E. T. Baldwin, G. B. Sancar, and A. Sancar, "Action mechanism of Escherichia coli DNA photolyase. II. Role of the chromophores in catalysis," *J. Biol. Chem.*, 1987.

[84] A. Hendrischk *et al.*, "A cryptochrome-like protein is involved in the regulation of photosynthesis genes in Rhodobacter sphaeroides," vol. 74, no. October, pp. 990–1003, 2009.

[85] J. C. N. Fong, K. Karplus, G. K. Schoolnik, and F. H. Yildiz, "Identification and characterization of RbmA, a novel protein required for the development of rugose colony morphology and biofilm structure in Vibrio cholerae," *J. Bacteriol.*, 2006.

[86] K. Hitomi *et al.*, "Functional motifs in the (6-4) photolyase crystal structure make a comparative framework for DNA repair photolyases and clock cryptochromes," *Proc. Natl. Acad. Sci.*, 2009.

Appendix A

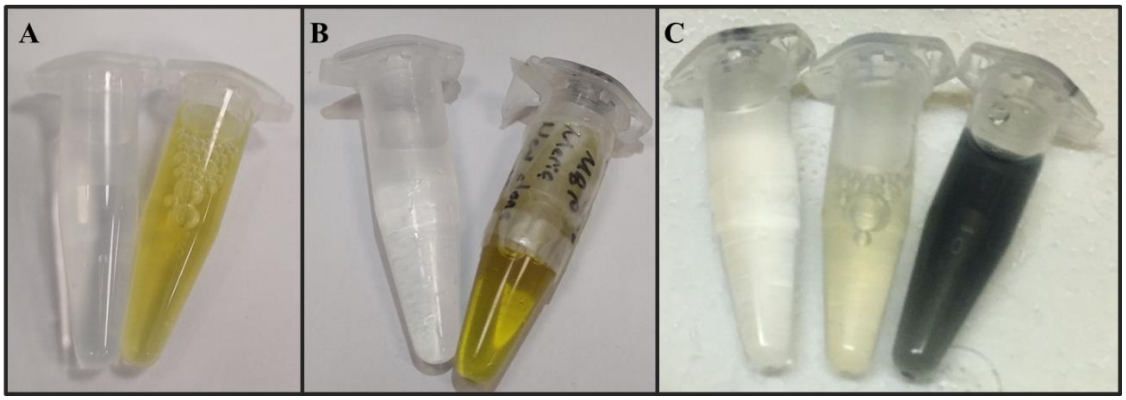

Figure 21. Color of purified Vc (6-4) FeS BCP-MBP fusion protein. (a) Left: Elution buffer, Right: protein containing fraction. (b) Left: Elution buffer, Right: purified protein concentrated by dialysis. (c) Left: Elution buffer, Middle: Vc (6-4) FeS-BCP fraction from a low yield purification experiment. Right: VcPhr containing fraction. Yellow color indicates the presence of oxidized FAD, brownish color indicates [4Fe-4S] cluster, and blue color indicates neutral FAD.